catalysts

MDPI

Review

Supported Ni Single-Atom Catalysts: Synthesis, Structure, and Applications in Thermocatalytic Reactions

Alina D. Nishchakova [1], Lyubov G. Bulusheva [1] and Dmitri A. Bulushev [2,*]

[1] Nikolaev Institute of Inorganic Chemistry SB RAS, 3 Acad. Lavrentiev Ave., 630090 Novosibirsk, Russia; nishchakova@niic.nsc.ru (A.D.N.); bul@niic.nsc.ru (L.G.B.)
[2] Boreskov Institute of Catalysis SB RAS, 5 Acad. Lavrentiev Ave., 630090 Novosibirsk, Russia
* Correspondence: dmitri.bulushev@catalysis.ru

Abstract: Nickel is a well-known catalyst in hydrogenation and dehydrogenation reactions. It is currently used in industrial processes as a homogenous and heterogeneous catalyst. However, to reduce the cost and increase the efficiency of catalytic processes, the development of single-atom catalysts (SACs) seems promising. Some SACs have already shown increased activity and stability as compared to nanoparticle catalysts. From year to year, the number of reports devoted to nickel SACs is growing rapidly. Among them, there are very few articles devoted to thermal catalysis, but at the same time, this subject is important. Thus, this review discusses recent advances in the synthesis, structure, and application of nickel SACs, mainly in catalytic hydrogenation/dehydrogenation reactions and in the dry reforming of methane. The collected and analyzed data can be useful in the development of novel nickel SACs for various processes.

Keywords: single-atom catalyst; nickel; hydrogenation; dehydrogenation; dry reforming

Citation: Nishchakova, A.D.; Bulusheva, L.G.; Bulushev, D.A. Supported Ni Single-Atom Catalysts: Synthesis, Structure, and Applications in Thermocatalytic Reactions. *Catalysts* **2023**, *13*, 845. https://doi.org/10.3390/catal13050845

Academic Editor: Carolina Belver

Received: 14 April 2023
Revised: 4 May 2023
Accepted: 4 May 2023
Published: 6 May 2023

1. Introduction

Nickel, the 28th chemical element of Mendeleev's periodic table of chemical elements, is relatively widespread; its prevalence in the Earth's crust is 0.009 wt% [1]. The study of the catalytic activity of nickel began in 1879 by the French chemists Paul Sabatier and Jean-Baptiste Senderens, and the reaction that first showed its activity, namely the direct one-stage hydrogenation of ethylene to ethane, is known as the Sabatier-Senderens reaction. Sabatier was the first to widely demonstrate the catalytic activity of nickel, which he described in detail in his famous book "Catalysis in Organic Chemistry" [2]. It seems that many researchers who have studied the catalytic reactions with this particular metal have heard Sabatier's famous description of a nickel catalyst: "It can be compared to a spirited horse, delicate, difficult to control, and incapable of sustainable work". However, few of them specify that later in his book, Sabatier determined that the pretreatment of nickel greatly affects its catalytic activity. Sabatier clearly formulated the conditions and features of the catalyst's preparation, and the reactions of hydrogenation and dehydrogenation of organic compounds served as the starting point for the development of nickel catalysts.

Nowadays, nickel-based catalysts are widely used both at laboratory and industrial scales. Ethylene carbonylation in the presence of nickel carbonyl makes it possible to synthesize propionic acid (Reppe reaction) [3], which, in turn, is widely used in the production of drugs (ibuprofen, etc.), plastics (for example, polyvinyl propionate), surfactants, and also as a preservative E280. The presence of the $Ni[(ArO)_3P]_4$ catalyst ensures the hydrocyanation of 1,3–butanediene followed by the isomerization of the reaction products to adiponitrile [4]. The Raney Ni catalyst is used in many hydrogenation reactions [5], for instance, in the conversion of benzene to cyclohexane, in the production of sorbitol from glucose, and in the production of amines from nitro-containing compounds. In the examples given, nickel, with the exception of Raney Ni, acts as a homogeneous catalyst, which is usually inferior to heterogeneous catalysts in industrial processes due to the difficulties associated

with separating the catalyst and the reaction mixture. However, homogeneous catalysts have an undeniable advantage since each Ni-containing molecule is a catalytically active center, which allows them to be used in a small concentration, in contrast to heterogeneous catalysts. To offset this shortcoming, the current development of heterogeneous catalysis is focused on single-atom catalysts (SACs).

The development of SACs is a trend of the last decade in modern catalysis, that is just beginning to gain momentum. Many scientists around the world are reporting that the use of catalytically active single atoms improves the efficiency of some reactions by increasing conversion, increasing selectivity to target products, and prolonging the operation of catalysts due to their exceptional stability. Carrying out a catalytic reaction on a specific single atom stabilized by a support makes it possible to reduce the loading of the metal as a whole. Such an approach allows one to reduce overall costs and save non-renewable resources (for example, the content of the most commonly used platinum group metals in the Earth's crust is only about 10^{-6}–10^{-8} wt% [1]). The change in catalytic activity is associated with the nature of active sites.

Figure 1 shows how metal-based catalysts can be classified by size, from bulk metal, which does not require the presence of a support, to single atom, which does. In each case presented, the surface atoms can catalyze the reaction; however, the particle surface structure, as well as the total number of metal atoms on the surface, will determine the catalytic activity. Since this review is devoted to nickel, we should consider its crystal—a face-centered cubic lattice [6]. In this structure, each bulk Ni atom has a coordination number of 12 (saturated coordination), while the surface atoms located in the center of the cube faces are bonded to eight atoms, the atom in the middle of the edge has a coordination number of five, and the nickel atom located at the corner of the lattice is connected to three atoms. Thus, the highest degree of unsaturation is observed for the corner surface atoms, which makes them energetically and often catalytically more attractive. However, this reasoning is applicable only to particles with more than 13 atoms, having at least one internal bond with the maximum saturation, and having the Ni crystal lattice. In the case of amorphous particles or somehow ordered clusters consisting of less than 12 atoms, bond unsaturation for each atom, especially for surface ones, will increase, reaching a maximum for a single atom. Having the highest surface energy, a single Ni atom, like any other metal, needs to be strongly stabilized on the support to prevent its migration for the purpose of binding (for example, agglomeration) in order to reduce the free surface energy. Thus, with the transition from bulk metal to a single atom, there is a loss of stability, often accompanied by an increase in the activity of the catalytic center due to an increase in the unsaturation degree.

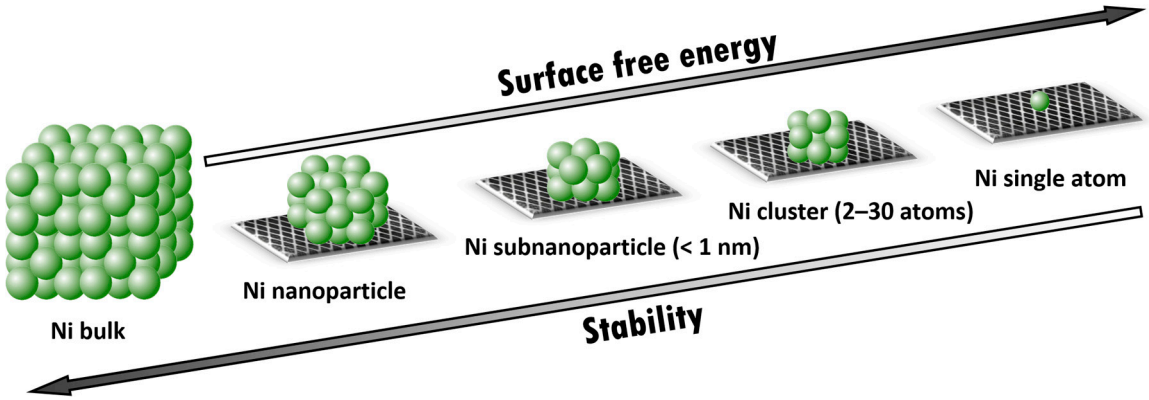

Figure 1. From Ni bulk to supported Ni single atom.

The study of metals in the atomic state is associated with difficulties caused by the resolution of characterization methods. Many reviews are devoted to the characterization of metal in a single-atom state [7–14]. In the simplest case, indirect confirmation can be

used based on a set of methods that confirm the presence of metal in the sample, but its absence in the form of bulk or nanoparticles. However, researchers most often use the three methods depicted in Figure 2: X-ray photoelectron spectroscopy (XPS), electron microscopy, and X-ray absorption fine structure (XAFS) spectroscopy. XPS can be used to determine the electronic state of nickel. The main binding energies for nickel in various oxidation states (from Ni^0 to Ni^{3+}), as well as the standard Ni *2p* spectrum, are shown in Figure 2 on the left. Using XAFS spectroscopy (Figure 2, on the right), it is possible to determine the nickel oxidation state (X-ray absorption near edge structure, XANES region) and atom environment (Fourier transform of extended X-ray absorption fine structure, EXAFS region). Figure 2 shows the Fourier transform of the EXAFS region of the studied and reference samples, from which, by correlating the positions of the main peaks, the local environment of the closest coordination spheres of the nickel atom can be observed. To determine the surrounding atoms, bond lengths, and coordination numbers, it is necessary to carry out additional fitting of the spectra. To directly show the monatomic distribution of the metal, the authors usually use electron microscopy (Figure 2, lower middle). Thanks to the resolution achieved by modern microscopes, the single metal atoms and the lattice in which they are located can be observed. Thus, by combining the three characterization methods presented, the resulting metal single atoms can be fully investigated, which is necessary to further establish the 'material-properties-application' relationship.

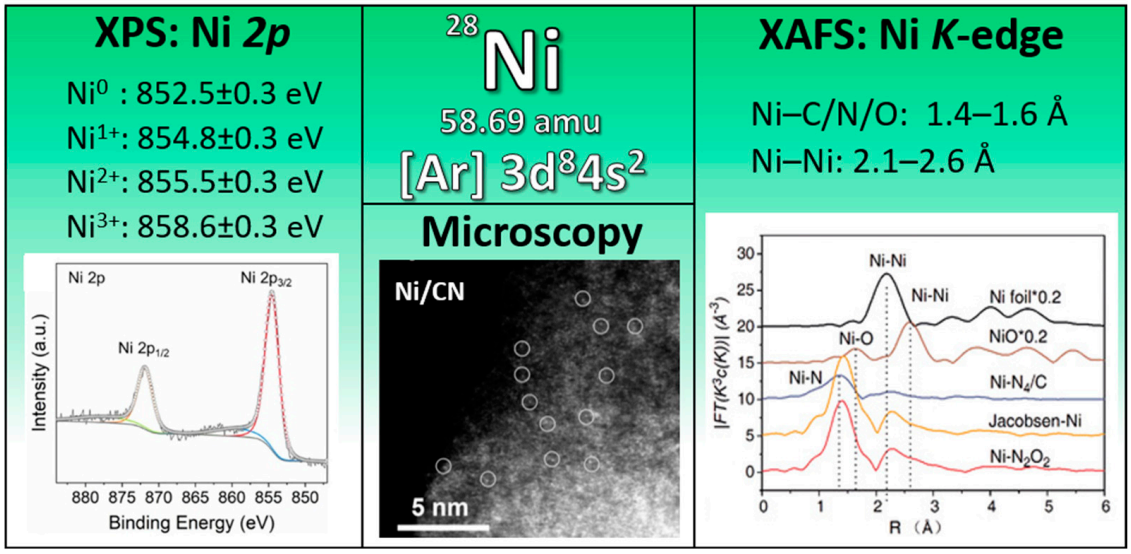

Figure 2. Some general information about the Ni element and characterization methods of Ni single−atom catalysts. XPS and XAFS spectroscopy data were taken from [15–24]. The examples of standard figures/images of the XPS Ni *2p* spectrum, high−angle annular dark−field scanning transmission electron microscopy (HAADF/STEM), and EXAFS Ni *K*−edge spectrum were adapted with permission from [19] (Copyright 2022, Wiley-VCH Verlag GmbH and Co. KGaA), [25] (Copyright 2020, the Royal Society of Chemistry), and [20] (Copyright 2020, Wiley-VCH Verlag GmbH and Co. KGaA), respectively.

Over the past few years, the number of publications devoted to Ni SACs has increased. More than half of them are related to the study of electrocatalytic reactions and corresponding density functional theory (DFT) calculations. This tendency is expected due to humanity's attempts to avoid the production of energy partially or completely by releasing it from non-renewable, non-ecofriendly oil and gas, while many advanced clean energy technologies require highly active catalysts to lower the energy barrier and increase the reaction rate with an efficient and stable route.

In this review, we discuss the use of nickel SACs in thermocatalytic reactions, mainly hydrogenation and dehydrogenation reactions, since Ni catalysts are very important for industry [3,5,26–29]. We do not discuss catalytic oxidation reactions or electrocatalytic

reactions. Before discussing applications, we present methods for the synthesis of catalysts containing Ni in an atomically dispersed state and establish the main parameters affecting the synthesis of densely populated Ni SACs.

2. Synthesis of Supported Ni Single-Atom Catalysts

An isolated atom possesses a high surface energy; therefore, under environmental conditions and, especially, harsh catalytic reaction conditions, it is susceptible to migration and agglomeration into clusters and nanoparticles. The catalytic properties of a catalyst strongly depend on its electronic state. Thus, the quality of the raw materials and each step that takes place with a catalytically active site during synthesis affect single atom formation and determine the resulting catalytic behavior. The methods for obtaining Ni SACs are very diverse and are selected depending on the choice of starting materials. Basically, all synthesis methods can be divided into two main groups: wet chemistry and pyrolysis.

2.1. Wet-Chemistry Methods

Wet-chemistry methods include impregnation (incipient) and precipitation, when various Ni-containing molecules (salts, complexes, etc.) are adsorbed or precipitated, respectively, from their solutions onto a prepared support material. Unfortunately, both of these methods are rarely used to synthesize Ni SACs. The nucleation and growth processes that occur during precipitation allow tuning the size of the resulting metal particles by changing various parameters, such as the pH of the solution, the Ni precursor, and precipitation agent concentration, temperature, etc. Due to the LaMer's model (Figure 3), the formation of Ni in the atomic state also strongly depends on the duration of synthesis, and, without an additional stabilization of atoms, self-nucleation and coalescence cannot be avoided.

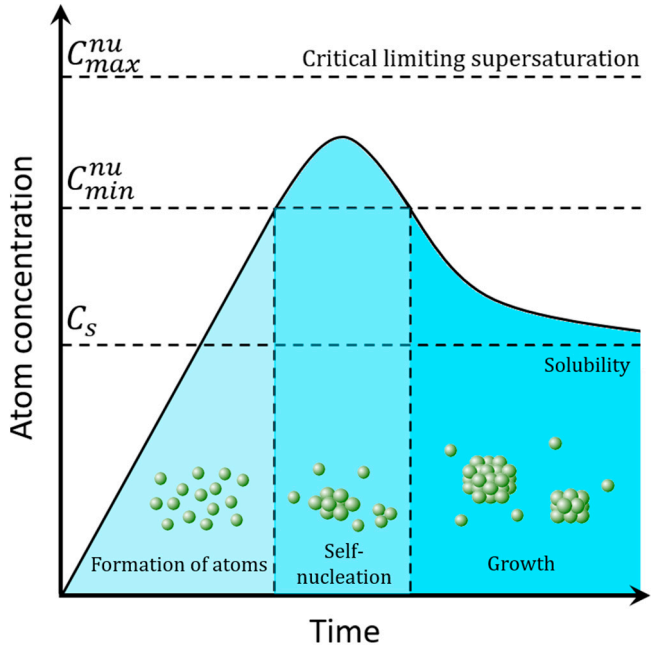

Figure 3. LaMer's nucleation model, where C_S is a concentration of supersaturation, $C^{nu}{}_{min}$ is a minimum concentration for nucleation, and $C^{nu}{}_{max}$ is a maximum concentration for nucleation. Reproduced with permission from [30]; Copyright 1950, American Chemical Society.

The same problem arises in the impregnation method for the synthesis of a Ni SAC, although some of the researchers mentioned below were able to level the low stability of the metal atoms by selecting a suitable support. Catalyst supports must have both sufficient surface area and centers to anchor single atoms to avoid their subsequent agglomeration into clusters and nanoparticles, as well as an exceptional combination of physical and chem-

ical properties required for a catalysis. Among those having the stated characteristics, one can distinguish nitrogen-containing carbon materials, successfully used for the synthesis of Ni SACs. Starting from the lowest Ni concentrations of 0.48 and 1 wt%, obtained by Buchele's [21] and Bulushev's [15] research groups, respectively, via impregnation with nickel acetate tetrahydrate solution, and ending with 4 wt%, reported recently by Lepre and co-authors [31]. Such a high Ni content of 4 wt% was achieved due to a number of factors, including the high nitrogen content (16 wt%) in the carbon support, the use of Ni bis(acetylacetonate) as a precursor, and the decomposition of the acid residue in air. Accordingly, isolated in the salt, Ni atoms were greatly stabilized by pyridinic nitrogen atoms of the support and oxygen atoms from acetylacetonate and air oxygen. The radial distribution functions revealed catalytically active Ni as Ni–$C_1N_1O_2$ sites. Thus, such Ni single-atom content is the highest reported for catalysts obtained by the impregnation method. Also, Wang et al. used MoS_2 nanosheets on carbon cloth to deposit 1.8 at% Ni [32]. Ni dichloride served as the Ni precursor, and the catalyst was formed in a reducing (H_2/Ar mixture) atmosphere. Atomic-resolution STEM images revealed bright spots that were associated with S-coordinated Ni at the nanosheet edge and at the hexagon center of the basal MoS_2 plane.

At the same time, the use of organic compounds to pre-stabilize Ni atoms can potentially result in a higher metal content. The impregnation method, which includes pre-stabilization of atoms, is called co-assistant impregnation. Since it is widely known that the pyridinic nitrogen functional group is temperature stable and can stabilize a metal atom, organic molecules containing it are successfully used. Two molecules of 1,10–phenanthroline contain four pyridinic nitrogen atoms, which ideally coordinate the Ni atom in the Ni–N_4 site. The complex can be deposited on the support surface and decomposed, retaining the coordination of metal [20,22]. According to the reported data, a temperature of 600 °C is required to obtain a Ni single-atom content of up to 5.3 wt% using Ni acetate tetrahydrate as the Ni precursor. Another organic compound containing pyridinic nitrogen, melamine, was used to form an atomically dispersed 2.6 wt% Ni catalyst from $NiCl_2 \cdot 6H_2O$ by heat treatment at 800 °C [23]. To coordinate the Ni atom, not only nitrogen atoms but both nitrogen and oxygen atoms are used. For instance, the Jacobsen's ligand was used by Wang and co-authors to strongly coordinate each Ni atom by two nitrogen and two oxygen atoms (Ni–O_2N_2), allowing 2 wt% of single-atom content [20]. It is noteworthy that each stabilizer, except for the latter one, required decomposition at a temperature of 600 °C and above, so carbon black, which has excellent thermal stability, was used as a support. However, the treatment temperature should be carefully selected since the use of temperatures above 800 °C leads to the breaking of the Ni–O bond, which was clearly observed by Rong et al. [33]. There, $NiCl_2 \cdot 6H_2O$ was mixed with cyanuric acid (O- and N-containing molecules) and 2,4–diamino–6–phenyl–1,3,5–triazine (N-containing molecules) and deposited on the carbon cloth. By annealing this mixture at different temperatures, the authors achieved different coordination of the nickel atom: the Ni–N_3O site obtained at 500 °C lost an oxygen atom in the form of a CO molecule during heat treatment at 800 °C, leading to the catalytically active Ni–N_3–V site (Figure 4).

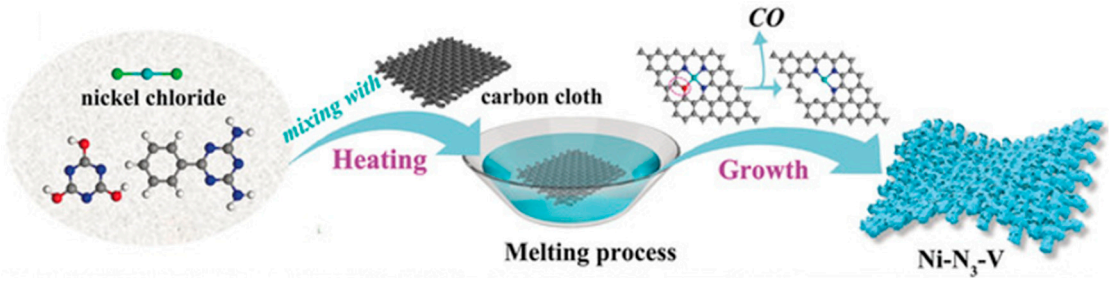

Figure 4. Illustration for the synthesis of Ni–N_3–V, adapted with permission from [33]; Copyright 2020, Wiley-VCH Verlag GmbH and Co; KGaA.

The above examples show that in the preparation of Ni SACs by impregnation method, one should wisely choose the appropriate (1) support, (2) Ni precursor or Ni precursor—stabilizer pair, and (3) pretreatment conditions. Due to that, some control over the metal atoms can be achieved, thus far leading to 5.3 wt% of Ni single-atom content.

2.2. Pyrolysis Methods

Despite the simplicity and possibility of achieving an atomic nickel dispersion, impregnation and precipitation methods often require post-synthetic acid treatment of catalysts to get rid of the resulting nickel nanoparticles. Careful selection of the conditions necessary to occupy a limited number of pre-created stabilization centers can still lead to a low concentration of Ni single atoms. Also, the content of 5.3 wt% of Ni single-atoms obtained so far does not satisfy the growing demands of consumers; researchers have to decrease the cost and complexity of the synthesis of SACs. One such approach is the sol-gel method. This method allows achieving the uniform chemical composition. Li et al. reported the synthesis of a catalyst with a 3.1 wt% content of Ni single atoms by mixing sucrose, $NiCl_2 \cdot 6H_2O$, and H_2SO_4 in water, thus dispersing Ni in the atomic state with hydroxide sucrose groups and initiating a polycondensation reaction in the presence of sulfuric acid [18]. The addition of excess amounts of NaCl created a template structure, which was occupied by the sol upon drying under cryogenic conditions. Subsequent annealing of the material obtained at 700 °C made it possible to create a carbon matrix on which pre-dispersed atomic nickel was stabilized as $Ni–O_4(OH)_2$ species. The NaCl template was removed with water. However, when using a template in the synthesis process under conditions different from those required for the sol-gel method, it is necessary to choose other templates. Thus, Liu and co-authors used MgO to distribute Ni in coordination with 1,10–phenanthroline [24]. This approach allowed for a Ni content of 7.5 wt%. The following removal of MgO to create a Ni/N-C catalyst required acid etching for several hours.

To obtain a higher Ni content, the surface areas of matrices for its dispersion should be larger, so metal-organic frameworks (MOFs) or their subclass, zeolitic imidazolate frameworks (ZIFs), are widely used. It is a three-dimensional material comprised of metal ions or clusters bound to organic ligands to form secondary building blocks. Often, the synthesis involves mixing zinc salt with 2–methyl imidazole solutions, which easily form an ordered 3D lattice. The introduction of nickel salts at the assembly stage allows their atoms to replace zinc in the lattice. An example of such an approach is the report by Yan et al., where various ratios of Ni and Zn nitrate hexahydrates were used [34]. The temperature and duration of decomposition depended on the Ni content in the sample in order to avoid Ni aggregation and, thus, the formation of nickel nanoparticles, which was completely prevented for all catalysts. During pyrolysis, 2–methyl imidazole is carbonized and Zn is mostly evaporated, forming a defective carbon-nitrogen matrix. The coordination of Ni atoms was calculated as $Ni–N_{2–3}$, and the Ni content corresponded to 5.44 wt%. However, Zn anchored on the carbon surface in an amount of ~3 wt% was still observed using XPS and inductively coupled plasma-optical emission spectrometry. Thus, it is necessary to correctly select the thermal decomposition conditions, which allow not only controlling the atomic dispersion of nickel but also removing zinc from the resulting catalyst. Wu and co-authors reported the synthesis of catalysts using dicyandiamide instead of 2–methyl imidazole as an organic ligand (Figure 5a) [35]. A mixture of Ni and Zn salts with dicyandiamide was treated in N_2 flow at three different temperatures: 350 °C, 650 °C, and 900 °C. This was done in order to gradually synthesize the g-C_3N_4 support on which metal atoms could be atomically stabilized and then to decompose the support into N-doped carbon material. Interestingly, when applying a thermal decomposition profile, the formation of encapsulated Ni nanoparticles was observed. Thus, a further increase in temperature to 900 °C initiated the growth of N-doped carbon nanotubes (CNTs). Owing to the extended surface of nanotubes and the presence of pyridinic nitrogen inherited from decomposed dicyandiamide and subsequent g-C_3N_4, which is still stable under the given synthesis conditions, nickel atoms were fixed in the nanotubes lattice in the form of $Ni–N_4$ species

directly during their growth. The obtained metal particles were removed by treatment with sulfuric acid, although a large amount of Ni nanoparticles was still observed in the samples. The achieved content of Ni single atoms in the catalysts was as high as 8.9 wt%, according to XPS. Thus far, only one study has reported a higher Ni single-atom content of 20 wt% [36]. In this work, Ni was also atomically anchored on N-doped CNTs (Figure 5b). Interestingly, the same temperature profile as in [35] was applied to treat a mixture of Ni acetylacetonate with dicyandiamide, thus confirming the importance of the catalyst synthesis route.

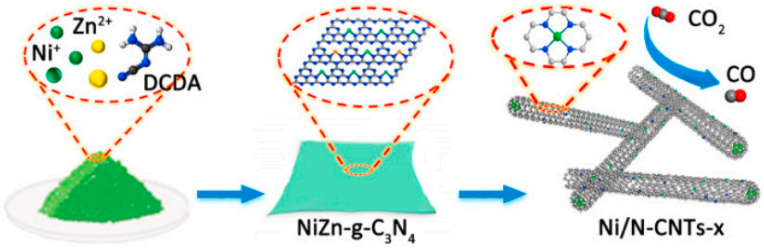

(**a**)

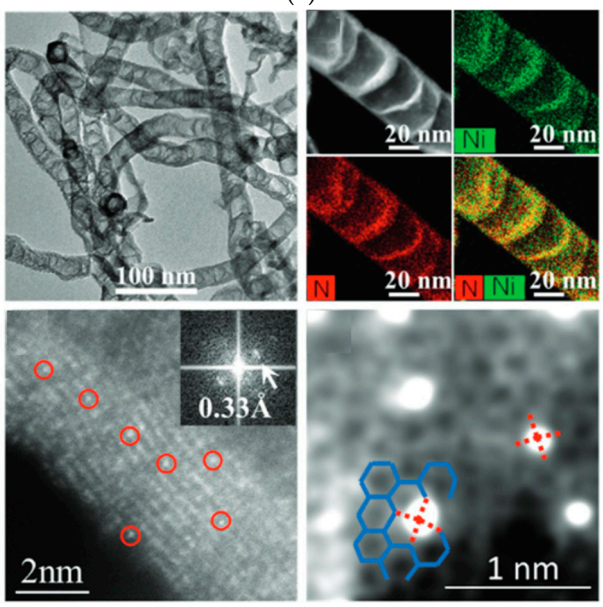

(**b**)

Figure 5. (**a**) The scheme of the synthesis of Ni/N–CNT catalysts reproduced with permission from [35], Copyright 2022, Elsevier B.V.; (**b**) HAADF/STEM images and elemental mapping of Ni/N–CNTs reproduced with permission from [36], Copyright 2019, Wiley-VCH Verlag GmbH and Co. KGaA.

Therefore, the simultaneous synthesis of both Ni single-atoms and the catalyst support is a more complex and expensive approach, but it allows one to achieve a significantly higher Ni content than using wet-chemistry methods. Whether or not the features of the catalyst's synthesis mentioned above clearly show that a very thoughtful approach to synthesis conditions selection is always needed.

3. Structure of Supported Ni Single-Atom Catalysts

Nowadays, Ni SACs are widely studied. The progress achieved over the past five years in the content of Ni single atoms on various supports is demonstrated in Table 1. The coordination of the Ni atom and the bond lengths in the single-atom sites are also given, since they determine the nature of the active site and the catalytic reactivity. Therefore, the latter could be tailored based on knowledge of the nature of the active site.

Table 1. Studied Ni SACs and their structural features, where 'V' in Ni coordination means vacancy.

Year	Support Material	Ni Content	Ni Coordination	Bond Length [a], Å	Reference
2018	N–doped holey graphene framework	0.05 at% [b]	Ni–N_4	1.89	[37]
	N–doped graphene	0.41 at% [c]	Ni–N_4O_1	1.87 and 2.19	[38]
	N–doped graphene	0.8 wt% [b]	Ni–N_4	1.86	[39]
	N–doped carbon	2.83 wt% [d]	Ni–N_4	Not given	[40]
	N–doped graphene	4.6 wt% [b]	Ni–N_4	1.861	[41]
	N–doped porous carbon	5.44 wt% [e]	Ni–N_2V_2	1.88	[34]
	N–doped carbon	7.5 wt% [b]	Ni–N_5	1.90 and 2.14	[24]
	N–doped carbon	9.5 wt% [f]	Ni–N_4	1.838	[42]
	N–doped carbon nanotubes	20 wt% [g]	Ni–N_4	1.86	[36]
	N–doped carbon nanotubes	20.3 wt%	Ni–N_4	1.86	[43]
	N–doped carbon nanosheet	Not given	Ni–N_4	Not given	[44]
	N–doped graphene	Not given	Ni–N_3O_1	1.87 and 2.10	[45]
	N–doped carbon	Not given	Ni–N_4	1.89	[46]
	Graphdiyne	0.278 wt% [d]	Ni–C_{12}	2.05	[47]
	Defective graphene	1.24 wt%	Ni–C_4 and Ni–C_5	1.78 and 1.99	[48]
	MoS_2 nanosheets array on carbon cloth	1.8 at% [b]	Ni–S_x	Not given	[32]
	Hierarchical MoS_2 nanosheets supported on carbon matrix nanofibers	2.7 wt% [e]	Ni–S_5	2.19	[49]
2019	N–doped carbon cloth	0.48 μg·cm^{-2} 0.52 μg·cm^{-2}	Ni–N_3V_1 Ni–N_4	1.84 1.88	[33]
	N-doped carbon matrix on carbon nanotubes	0.087 wt% [b]	Ni–N_2C_2	1.86 and 2.73	[50]
	Porous carbon nanosheets	0.2 wt% [e]	Ni–N_3S_1	1.85 and 2.33	[51]
	Carbon nanotubes	0.27 wt% [d]	Ni–N_4	Not given	[52]
	N atoms decorated hollow carbon matrix	1.27 wt% [d]	Ni–N_4	1.91	[53]
	Covalent triazine framework	2.4 wt% [c]	Ni–N_4	1.845	[54]
	N–doped graphene aerogel	2.6 wt%	Ni–$N_{x<4}$	Not given	[23]
	N–doped porous carbon	4.4 wt% [e] 4.9 wt% [e]	Ni–N_3 Ni–N_4	1.84 1.86	[55]
	N–doped black carbon	5.32 wt% [e]	Ni–N_4	Not given	[22]
	N–doped carbon nanotubes	6.63 wt% [e]	Ni–N_x	Not given	[56]
	N–doped graphene	Not given	Ni–N_4	1.81 and 1.97	[57]
	N–doped carbon	Not given	Ni–N_4	1.864	[58]
	CeO_2	2.5 wt%	Ni–O_3Ce_3	1.89 and 2.94	[59]
	Hydroxyapatite	2.58 wt% [b]	Ni–O_6	2.05	[60]
	Amorphous Y_2O_3 nanosheets	3.9 wt% [b]	Ni–O_3	Not given	[61]
2020	Carbon spheres	0.37 % [f]	Ni–N_4	2.02	[62]
	Honeycomb–like carbon	0.77 at% [c]	Ni–N_4	1.96	[63]
	N–doped hollow carbon	0.10 wt%	Ni–N_4	1.92	[64]
	N–doped carbon	0.12 wt% [e]	Ni–N_4	1.98	[65]
	Carbon nanotubes	0.17 wt% [e] 0.21 wt% [e]	Ni–N_3V_1 Ni–N_4	1.844 1.898	[66]
	Carbon nanotubes	0.27 wt% [e]	Ni–N_4	Not given	[67]
	N–doped carbon	0.48 wt% [e]	Ni–$N_{4–5}$	2.05	[21]
	N–doped graphitic carbon	0.5 wt% [h]	Ni–N_4	1.876	[68]
	Carbon nanotubes	0.76 wt% [d]	Ni–N_4	1.91	[69]
	N–doped carbon	0.872 wt% [b] 0.889 wt% [b] 0.917 wt% [b]	Ni–N_4C_1 Ni–N_2C_2 Ni–N_3C_1	1.91 and 2.13 1.87 and 2.13 1.86 and 2.11	[70]
	Carbon paper	1.04 wt% [e]	Ni–N_3S	1.879 and 1.939	[71]

Table 1. *Cont.*

Year	Support Material	Ni Content	Ni Coordination	Bond Length [a], Å	Reference
2021	Carbon membrane	1.3 wt% [e]	$Ni–N_4$	1.93	[16]
	N–doped carbon layers	1.61 wt% [b]	$Ni–N_3$	1.87	[72]
	Janus hollow graphene	1.9 wt% [b]	$Ni–N_4$	2.09	[73]
	N–doped carbon	2 wt% [e] 2.2 wt% [e]	$Ni–N_2O_2$ $Ni–N_4$	1.85 Not given	[20]
	Three-dimensional hierarchical carbon	4.2 wt% [e]	$Ni–N_4$	1.87	[74]
	Graphene–like carbon	3.1 wt%	$Ni–O_4(OH)_2$	2.05	[18]
	N–doped carbon	0.24 wt% [d] Not given	$Ni–N_4O_1$ $Ni–N_4$	1.87 1.87	[75]
	Porous carbon nanosheets	0.5 wt% [e]	$Ni–N_1N_2S_1$	1.91, 2.06, and 2.03	[76]
	N–doped porous carbon	0.6 wt% [e]	$Ni–N_5$	1.92	[77]
	N–doped carbon	0.85 wt % [b] 1.06 wt% [b]	$Ni–N_3$ $Ni–N_4$	1.86 1.88	[78]
	N–doped porous carbon	1 wt%	$Ni–N_4$	2.00	[15]
	N–doped carbon	2.1 wt% [e]	$Ni–N_4$	1.89	[79]
	N–doped graphene	2.14 wt% [e]	$Ni–N_2$	1.83	[80]
	N–doped carbon	3.3 wt% [b]	$Ni–N_{3,4}$	1.85	[81]
	Reduced graphene oxide	1.4 at%	$Ni–O_x$	Not given	[82]
2022	N–doped carbon	0.51 at% [g]	$Ni–N_4$	1.93	[83]
	N–rich carbon hosts	1.1 at% [c]	$Ni–N_2O_2$	1.85 and 1.99	[84]
	N-doped carbon	Not given	$Ni–N_4O_1$	1.96 and 2.27	[85]
	Carbon nanotubes	0.4553 wt% [e]	$Ni–N_4$	1.887	[86]
	N–doped carbon matrix	0.51 wt% [e]	$Ni–N_4O_1$	1.94 and 1.90	[87]
	N–doped carbon	1.0 wt% [b]	$Ni–N_4$	1.84	[88]
	N–doped carbon	1.5 wt% [b] 3.3 wt% [b]	$Ni–N_5$ $Ni–N_4$	1.91 and 2.11 1.85	[89]
	N–rich carbon	1.6 wt% [e]	$Ni–N_4$	1.88	[90]
	N–rich carbon	1.66 wt% [e]	$Ni–N_4$	Not given	[91]
	N–doped carbon	Not given 1.89 wt% [b]	$Ni–N_4$ $Ni–N_5$	1.91 1.88	[92]
	Three-dimensional carbon material	2.20 wt% [d]	$Ni–N_3S_1$	1.89 and 1.94	[93]
	N–doped carbon	2.37 wt% [e]	$Ni–N_4$	1.86	[19]
	N–doped carbon	3.7 wt% [e]	$Ni–C_3N_1$	1.88 and 2.00	[94]
	N–doped carbon	4 wt% [e]	$Ni–C_1N_1O_2$	1.777, 2.045, and 2.925	[31]
	N–doped carbon	9.15 wt% [f]	$Ni–C_2N_2$	1.90 and 2.07	[95]
	S/N–doped carbon spheres	1.1 wt% [e]	$Ni–N_4$	1.88	[96]
	N,B co–doped porous carbon	1.5 wt% [e]	$Ni–N(B)_4$	1.89	[97]
	MoS_2 nanosheets	1.4 wt%	$Ni–S_3$	2.23	[98]
	TiO_2	0.4 wt% [b]	$Ni–O_{3–4}$	2.04	[99]
	CeO_2 nanospheres	1.0 wt% [e]	$Ni–O_3$	2.02	[100]
	$\gamma–Al_2O_3$	2.5 wt%	$Ni–O_4$	2.02	[101]

[a] According to EXAFS fitting data. [b] Ni content measured by inductively coupled plasma-atomic emission spectroscopy. [c] Ni content measured by XPS. [d] Ni content measured by inductively coupled plasma-mass spectroscopy. [e] Ni content measured by inductively coupled plasma-optical emission spectroscopy. [f] Ni content measured by inductively coupled plasma. [g] Ni content measured by energy-dispersive X-ray spectroscopy. [h] Ni content measured by X-ray fluorescence.

Above, we briefly discussed the dependence of the stability of Ni particles and clusters as compared to bulk Ni and determined that, when going to single atoms, the increased activity may coexist with low stability (Figure 1). However, many authors report high stability of catalysts in which nickel atoms are stabilized by nitrogen. Earlier, Bulushev and Bulusheva [102] compared the binding energies of various metal atoms with two and four pyridinic nitrogen atoms in a double vacancy of the graphene lattice ($M–N_2C_2$ and

M–N_4, respectively) and at the graphene edge (M–N_2) (Figure 6a). In the case of nickel, it can be seen that the binding energy of the Ni atom to the bulk metal (M–M_n) and in the Ni–N_2 site is approximately equal to 4 eV. However, when nickel is located in a graphene double vacancy, the binding energy in the Ni–N_2C_2 and Ni–N_4 configurations increases significantly to 10–11 eV, which is the highest among the considered metals. Such an increase in energy indicates the extreme energy benefit of the formation of these sites and also confirms their stability, which is observed in practice. As can be seen from Table 1, most of the Ni atoms in the single-atom state are bonded to several (up to four or five) nitrogen atoms with an average distance of 1.89 Å, which indicates a structure close to that of Ni phthalocyanine (1.90–1.91 Å) [103] or Ni porphyrin (1.95 Å) [104]. However, there are reports about distances greater than 2.00 Å [15,21,62,73]. It is noteworthy, that in all these works, the supports used are carbon materials contained regions with a curved structure (porous carbon, carbon spheres, etc.). Figure 6b,c clearly demonstrates how the Ni–N bond length in the Ni–N_4 site changes upon the transition from a flat to a curved structure. Regardless of the obtained bond lengths, the Ni–$N_{3–4}$ sites are highly stable up to at least 600 °C in an inert atmosphere [33,105] or even in harsh conditions of hot acidic solution and high pressure [24]. Thus, the areas of their potential application are significantly expanded.

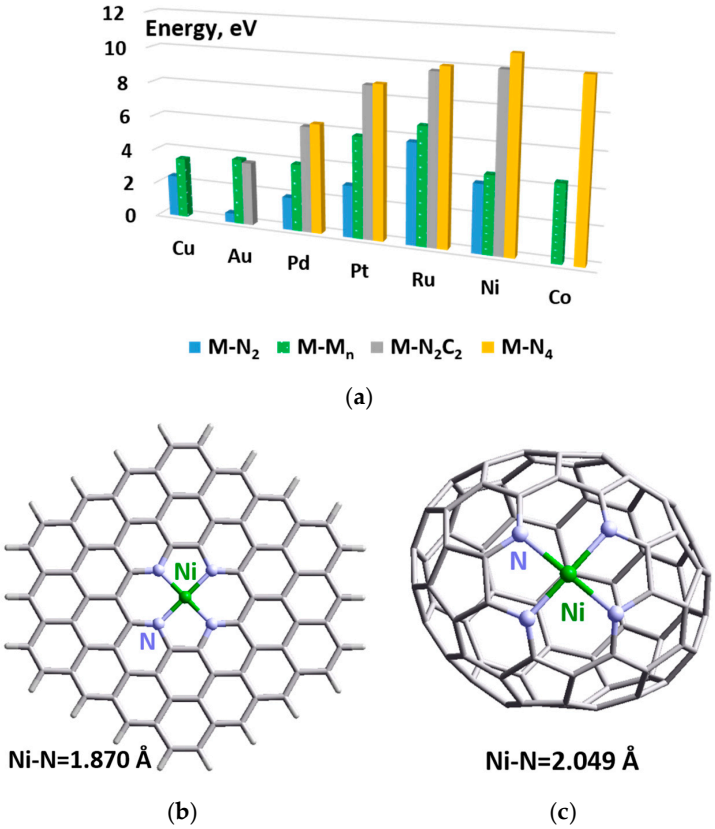

Figure 6. (**a**) Cohesive energies (M-M_n) and binding energies of single metal atoms on an N-doped graphene sheet, adapted with permission from [102] (Copyright 2022, Taylor and Francis), where M is metal; flat (**b**) and curve (**c**) models of carbon surfaces with Ni attached to N-terminated double vacancies, adapted with permission from [17]; Copyright 2023 by the Authors.

Table 1 shows that carbon, oxygen, and sulfur atoms can also, together with nitrogen atoms, stabilize nickel atoms on carbon supports, and in such sites, Ni–O, Ni–S, and Ni–C bonds are usually longer than those of Ni–N. When the Ni atom is stabilized only by carbon atoms, the average Ni–C bond length is 1.78 Å in the Ni–C_4 site [48]; however, with an increase in the coordination number or stabilization by different atoms, the Ni–C bond

length increases up to 2.05 Å [47,48] and even to 2.13 Å [70]. In turn, the length of the Ni–S bond changes from 2.2–2.3 to 1.94 Å [49,51,71,93], while the average Ni–O bond length, regardless of the support and coordination numbers, is 2.0–2.1 Å. As already mentioned in the section 'Synthesis of supported Ni single-atom catalysts', the stabilization of the nickel atom by both nitrogen and oxygen atoms on a carbon material limits the stability of the Ni–O bond to 800 °C [33]. However, when using a support based on metal oxide (CeO_2, Al_2O_3, etc.), this temperature decreases to 600 °C [59,101] or even lower [100]. In turn, catalysts containing Ni single atoms stabilized only by carbon or sulfur atoms have been used mainly for low-temperature electrochemical reactions; therefore, it is difficult to assess the conditions for their stable operation in thermal catalytic reactions, which usually demand higher temperatures. Although, according to the synthesis conditions, Ni on a defective graphene support is able to withstand temperatures up to 750 °C in a reducing atmosphere, as well as in an acidic environment at room temperature within two days [48], and on a MoS_2 support up to 300–600 °C also in a reducing atmosphere [32,49] and up to 900 °C in Ar [98]. Interestingly, a Ni single atom can be located above the MoS_2 layer [32,98] or can replace the Mo atom [49]. In the former case, the Ni atom is coordinated by three sulfur atoms, and this arrangement was suggested using HAADF/STEM imaging (Figure 7a). Single-dispersed bright spots in the images are explained by the location of Ni atoms above Mo atoms [98]. The EXAFS data was also well fitted with the Ni–S_3 structure. The incorporation of Ni into the MoS_2 lattice was revealed from the EXAFS data, which determined that the first coordination sphere of Ni consists of five S atoms on average [49]. This configuration of Ni was confirmed by good agreement between the experimental XANES Ni *K*-edge spectrum and the theoretical spectrum plotted for Ni replacing Mo (Figure 7b). In both configurations, the Ni–S bond is shorter than the Mo–S bond.

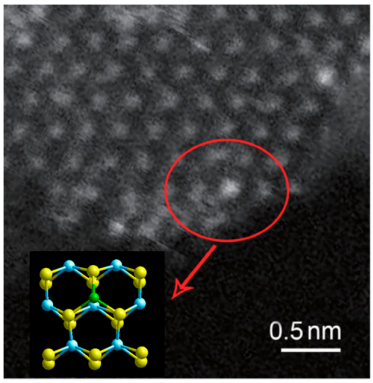

(**a**)

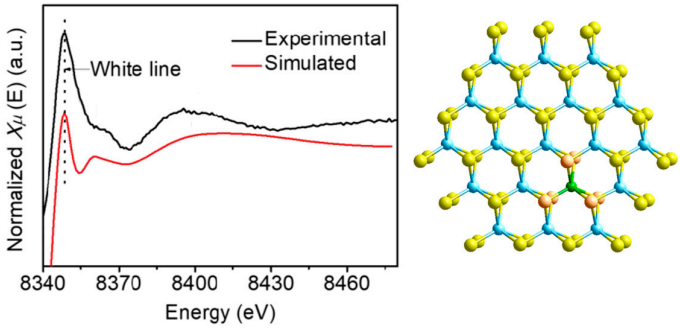

(**b**)

Figure 7. (**a**) HAADF/STEM image of Ni/MoS_2 with simulation inset; and (**b**) comparison between the Ni *K*-edge XANES experimental spectrum of Ni/MoS_2 and the theoretical spectrum calculated with the depicted structure. Nickel, molybdenum, and sulfur atoms are represented by green, light blue, and yellow balls, respectively. Adapted with permission from [98] (Copyrights 2023, Springer Nature) and [49] (Copyrights 2018, Wiley-VCH Verlag GmbH and Co. KGaA.), respectively.

4. Application of Supported Ni Single-Atom Catalysts

In the Introduction section, we briefly discussed the historical and modern applications of Ni-based catalysts, which are mainly related to the catalysis of hydrogenation and dehydrogenation processes. When discussing catalysts for such reactions, one cannot fail to mention the competition between palladium and nickel, which was well covered in a recent review by Chernyshov and Ananikov [106]. Indeed, being one under the other in the same group of the periodic table, these metals are analogues; however, the difference in the periods causes differences in redox potentials and the availability of different oxidation states, which provides outstanding opportunities for Ni catalysis for complex multistep transformations and the discovery of new catalytic reactions. Thus, we will consider both the theoretical and practical results of using Ni SACs in various hydrogenation and dehydrogenation reactions. It should be noted that the development of Ni SACs' application field is not much different from the historical ones for Ni bulk and Ni nanoparticles: this is the breaking of X–H bonds, where X is various atoms, for example, C or O, and H is a hydrogen atom. In this regard, for convenience, we will further consider separately the activity of heterogeneous catalysts based on Ni single atoms in breaking various X–H bonds, and we will start with the C–H bond.

4.1. C–H Activation

Currently, the most common catalysts for the activation of C–H bonds are Ni-based catalysts. The activity of nickel is associated with the presence of an unfilled *d* orbital, which can accept the σ electron of the C–H bond, thus weakening or breaking it [107]. Such an approach to the activation of hydrocarbons can facilitate cross-coupling reactions, leveling the disadvantages known for this reaction: the use of an expensive catalyst (Pd-based), the presence of several stages of pre-functionalization, which entails a multi-stage reaction, and the presence of by-products. However, the activation of the C–H bond also has its drawbacks, in particular, high reaction temperature and high metal loading are needed. The best-known nickel-catalyzed reaction involving C–H activation is the dry reforming of methane (DRM).

Dry Reforming of Methane

DRM is a process for the simultaneous synthesis of H_2 and CO (syngas) via the conversion of carbon dioxide and methane. Even though this reaction may not actually involve hydrogenation and dehydrogenation, its mechanism includes the C–H bond cleavage as an important step of the reaction. The general reaction (1) describing this process is endothermic with a standard enthalpy of 247 kJ mol^{-1} and, therefore, requires high temperatures (>500 °C) [59,60,108].

$$CH_4 + CO_2 \rightarrow 2CO + 2H_2 \quad (1)$$

The mechanism of this reaction has been thoroughly studied [109,110]. The reaction begins with the adsorption of a methane molecule on the catalytically active center (2), followed by its activation (3), which is the rate-determining stage of the reaction [111,112]:

$$CH_4(g) + cat \rightarrow CH_4^* \quad (2)$$

$$CH_4^* \rightarrow CH_3^* + H^* \quad (3)$$

where '(g)' stands for the gas phase and '*' here and below in the text means the adsorbed species. The methane molecule is a highly symmetrical nonpolar molecule, which should be considered when choosing a catalyst. As shown in the literature [113], the adsorption of methane on a metal single-atom site occurs due to the hybridization of bonding orbitals of the methane with antibonding orbitals of the metal and vice versa. It should be noted that a support on which metal single atoms are located may also play a role in methane adsorption. The stability of a metal atom is ensured by the strength of its bonding with a support, which is related to overlapping their orbitals. The lengthening of the C–H

bond, leading to its further cleavage, depends on the adsorption energy of methane and on the charge given back from metal. This bond elongation is most noticeable for the Ni atom, which is the rationale for the effectiveness of Ni SACs in the DRM reaction. Indeed, according to the reports of the past few years [114,115], Ni single-atom sites exhibit superior activity, in particular, as compared to Ni nanoparticles. However, their use often leads to catalyst deactivation, which is associated with the formation of carbon as a result of the Boudouard reaction (4) and the complete cracking of methane (5), catalyzed by nickel [110].

$$2CO \rightarrow CO_2 + C \quad (4)$$

$$CH_4 \rightarrow C + 2H_2 \quad (5)$$

It is interesting that the equilibrium in the Boudouard reaction can be shifted towards the formation of CO if the chosen support can donate electrons to the nickel atom or Lewis basic sites, which are attractive for CO_2 adsorption, are introduced into the catalyst. The former factor was widely studied in [107], where Ni nanoparticles supported by CeO_2 were used as a catalyst after a reduction in hydrogen. As a result of the reduction, oxygen vacancies were formed, which easily released free electrons. These free electrons increased the *d*-electron density on the nickel atoms. Such electron-saturated atoms prevented the migration of σ–electrons of the CH_4 molecule to the *d* orbital of the Ni atom, thereby reducing the adsorption of CH_4 and, thus, the degree of carbon deposition, and also increasing the adsorption of CO_2 due to including its unoccupied π–orbital in the bonding (Figure 8).

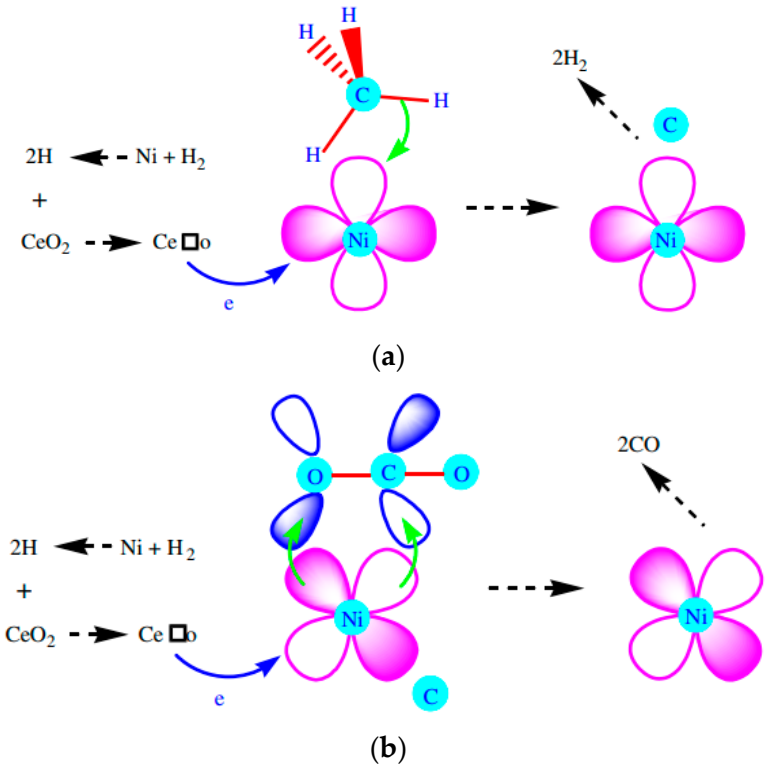

Figure 8. Schematic diagram of (**a**) carbon deposition and (**b**) carbon elimination over Ni/CeO_2 catalyst. Adapted with permission from [107]; Copyright 2002, Springer Nature.

Quite recently, these assumptions were partly confirmed for a similar $Ni/M–CeO_2$ system, containing Ni single atoms and a support modified with Mg, Co, or Zn [114]. In this case, CO_2 molecules were adsorbed on oxygen vacancies generated due to the presence of metal cations, whose ionic radius is smaller than that of Ce^{4+}. The carbon dioxide molecule dissociated into carbon monoxide and surface active oxygen, which easily removed the

deposited carbon, thereby maintaining high catalyst activity for more than 150 h at 800 °C. A similar effect was achieved by Ni and Ce co-doping of a hydroxyapatite support [60] and co-anchoring of Rh and Ni atoms on a CeO_2 support [59], showing in the latter case a decrease in the temperature of the catalytic process to 600 °C while the selectivity and stability stayed high. Interestingly, the authors of the latter work also reported that the recombination of H* into a hydrogen molecule occurred on Rh atoms, despite the fact that the process of breaking the C–H bond occurred on nickel atoms. In addition, ZrO_2 possesses the same properties of producing oxygen vacancies [116]. Thus, the first way to modify Ni SACs is based on the selection of supports containing a large number of oxygen vacancies, which are considered to be closely linked to the content of surface adsorbed oxygen species.

The second way to modify the catalyst by introducing additional basic centers into it is to add a metal and/or its oxide to the support. The creation of such centers will enhance the chemisorption of CO_2 on them [109]. As for the Zr and Ce atoms mentioned above, their addition to oxygen-containing supports also increased the mobility of oxygen ions on the surface, making Ni catalysts more stable [117]. As for other metals, there is a report of better catalytic activity and stability of Ni catalysts for 40 h at 700 °C, in which the support was partially coated with MgO [118]. Interestingly, such doping initiated better Ni dispersion on the support surface. However, this method did not work when using MgO as a support for Ni single-atoms [119] because of the weak bonding of Ni atoms with the support, methane, and carbon dioxide, as well as the low adsorption energy of reaction intermediates on the active site, which prevented the reaction.

The use of SACs, including Ni catalysts, is not sufficiently developed since this is a rather young area of catalysis. In this regard, there is no confirmation/denial in the literature of the promotion of the DRM reaction previously obtained for Ni nanoparticles in the case of single atoms (adding K [120], Ca [121], Fe [122], Sr [123] or using CaO, BaO [124], La_2O_3 [125], etc. as supports [126,127]). However, significant progress is expected in this field.

4.2. H–H Activation

Hydrogen is the simplest molecule, and its properties are the most studied. Since this pure resource is available in abundance at a very low cost, catalytic hydrogenation is a mainstream technology in both research and industry. Molecular hydrogen is not very active under ambient conditions, but many positively charged transition metal atoms are capable of bonding and activating H_2. As is well known, bulk Ni and Pd have a very strong hydrogen adsorption affinity, can easily form metal hydrides, and are widely considered good catalysts due to their excellent hydrogen solubility, corrosion resistance, and diffusivity. As indicated in the literature, the adsorption energy of the hydrogen molecule on the Ni single atom [128,129] is higher than that on bulk Ni [130]. The initiation of the hydrogenation reaction most often occurs with the dissociation of the hydrogen molecule. Homolytic decomposition yields adsorbed H* atoms, while heterolytic decomposition produces partially charged $H^{\delta+}$ and $H^{\delta-}$ species. The type of decomposition, the energy barrier, and the overall energy profile of the reaction strongly depend on the structure of the catalytically active Ni site. For example, according to DFT calculations of a catalytically active Ni atom coordinated to three and four carbon atoms in single and double graphene vacancies, H_2 dissociation is an endothermic process with energy barriers of 0.69 and 0.33 eV, respectively [131]. As can be seen, the dissociation of the adsorbed H_2 is an energy-consuming process [128,131,132]. However, with an increase in the number of Ni atoms to three in a catalytically active site, the dissociation is almost barrier-free [130]. Interestingly, a similar effect was observed when considering the reverse reaction, where the recombination of hydrogen atoms into a molecule took place [133]. After decomposition, hydrogen atoms can spontaneously migrate to support atoms. This effect is called the hydrogen 'spillover' process, and it may take place in the metal-carbon support system [134]. Such behavior, in particular, was observed for some nitrogen-containing systems [128] and also

for MoS_2 [132]. For instance, the addition of Ni single-atoms on MoS_2 support causes an excess of electron density on the nearest sulfur atoms, thus enhancing their activity towards hydrogen adsorption [32,49]. Although the activation of a hydrogen molecule can also occur due to an increase in the H–H bond length after adsorption onto the Ni atom (Figure 9a). Furthermore, during the co-adsorption of the reagents on the metal atom, the breaking of this bond for the further course of the reaction will be easier. An example of such a hydrogenation pathway is CO_2 hydrogenation.

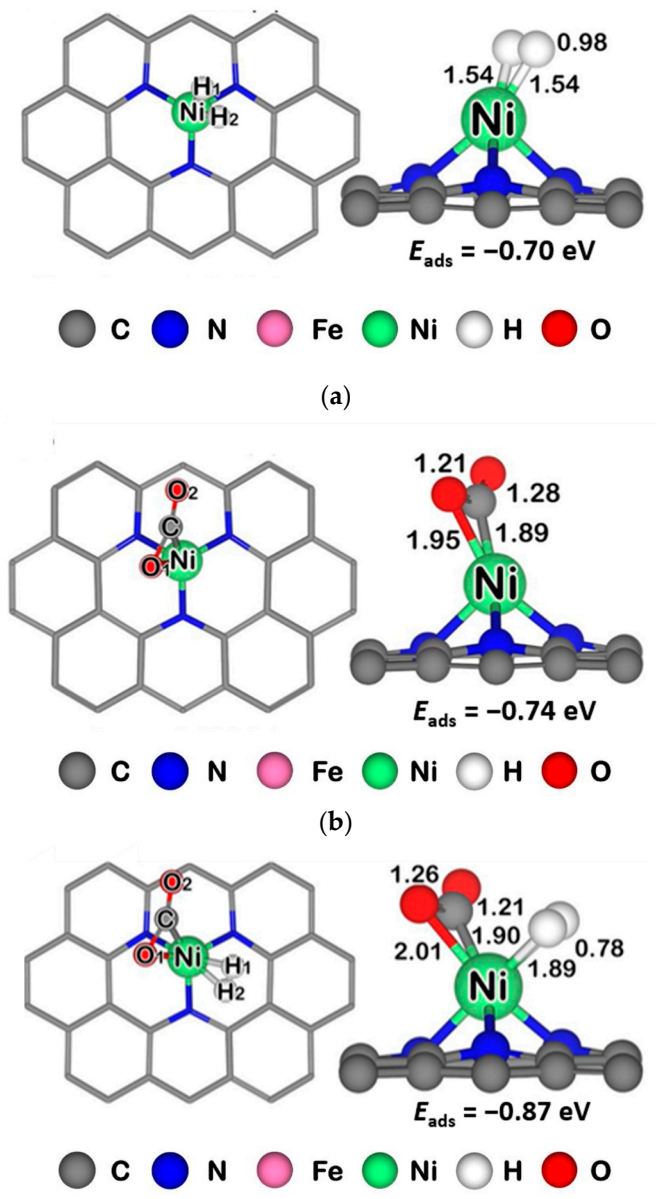

Figure 9. The most stable configurations (top and side views) and related adsorption energies (E_{ads}) for (**a**) H_2, (**b**) CO_2, and (**c**) both these molecules on the Ni–N_3 site in graphene. Adapted with permission from [129]; Copyright 2021, Elsevier B.V.

4.2.1. CO_2 Hydrogenation

It is widely recognized that capturing and utilizing carbon dioxide is a potentially effective strategy for reducing the concentration of CO_2 in the atmosphere and addressing the current environmental problems caused by massive CO_2 emissions. Most often, carbon dioxide is proposed to be processed into C1 fuels (Figure 10), for example, methane [135]

or formic acid [129,136] via hydrogenation reactions. Although the use of Ni SACs for both reactions has not yet been reported, there are a number of theoretical articles in the literature dealing with them. To produce methane, the initial reduction of CO_2 to CO is necessary. The adsorption of a CO_2 molecule occurs through the formation of a bond between the oxygen atom of a molecule and the metal atom [137,138]. However, there are reports about bidentate interaction through oxygen and carbon atoms (Figure 9b) [129,136,139]. Further decomposition of CO_2* to CO* and O* on the Ni single-atom site is impossible [140] or difficult in the absence of high temperatures (>800 °C) [141]. Therefore, for the dissociation of the C–O bond in carbon dioxide, a suitable support is usually selected that is capable of adsorbing and reducing CO_2 to the desired product [114]. The impossibility of producing methane on a Ni single atom is confirmed by Millet et al. [142], where, upon reaching a temperature of 350 °C, CH_4 appeared among the products, which was associated with the sintering of Ni into nanoparticles of about 10 nm in size. Notably, a small amount of methanol was also observed.

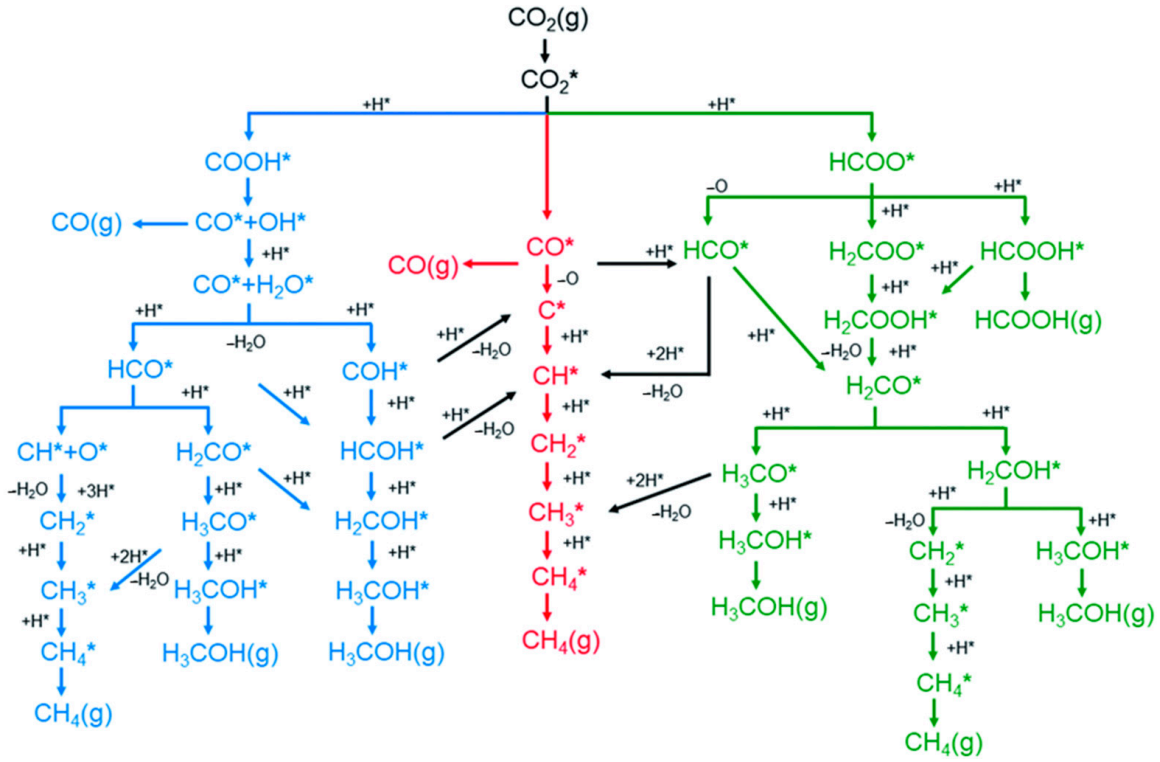

Figure 10. The reaction network of CO_2 hydrogenation towards CH_4, CO, CH_3OH, and HCOOH production over the supported Ni catalysts. Reproduced with permission from [141]; Copyright 2022, The Royal Society of Chemistry.

To obtain formic acid in the liquid phase as a result of hydrogenation of carbon dioxide, the presence of hydrogen is necessary (Figure 10). Interestingly, the presence of a hydrogen molecule or hydrogen atom adsorbed on a metal atom lowered the CO_2 adsorption energy but did not level it [136,138]. These results show that although CO_2 is repelled by adsorbed hydrogen, their co-adsorption is still energetically favorable (Figure 9c). Depending on which atom the CO_2 molecule interacts with hydrogen, formate HCOO* or carboxylate *COOH species can be formed as intermediates, and the formation of the former is more energetically favorable among Ni SACs on different supports [129,136,139]. The further formation of the HCOOH molecule was not considered in most articles. However, among them, Poldorn and co-authors took into account not only the formation of cis- and trans-isomers of formic acid but also the side reactions to form CO and H_2O [129]. Their calculations showed that trans-HCOOH can be obtained most easily as a result of this

reaction, while the course of the side reaction is energetically unfavorable. Thus, the production of formic acid on a Ni SAC has been performed electrochemically [31]; there are no reports that it can be produced via a thermal hydrogenation reaction. However, it has been shown that the production of formic acid is achievable on Ni nanoparticles at temperatures < 80 °C in the presence of an amine [143] or by hydrogenation of sodium bicarbonate at 200 °C [144].

4.2.2. C_2H_2 Hydrogenation

Acetylene hydrogenation is an important industrial process for purifying ethylene produced by thermal cracking of naphtha and containing trace amounts of C_2H_2, which can lead to poisoning of a C_2H_4 polymerization catalyst and reduce the quality of the resulting product. It should be noted that the acetylene molecule is nucleophilic, which suggests its preferential interaction with a positively charged catalyst site. Thus, the acetylene molecule is coordinated to a Ni atom by carbon atoms having π–electrons. Zhuo et al. noted that the adsorption of C_2H_2 is much easier than the adsorption of H_2 [131]; the process of acetylene adsorption is so energetically favorable that the question of a partial loss of the number of catalytically active metal centers is raised in the literature [145]. It was noted that the presence of nitrogen atoms near the metal reduces the adsorption energy of acetylene due to partial electron transfer from C_2H_2 to nitrogen atoms through the metal atom.

However, the nucleophilicity observed in acetylene is also present in the ethylene molecule obtained as a result of the reaction, which contributes to an increase in the desorption energy as compared to ethane, the end product of the C_2H_2 hydrogenation. The challenge of carrying out this reaction and choosing catalysts and conditions is to increase the selectivity for ethylene as the desired product and, accordingly, decrease it for ethane. Riley et al. [146] synthesized Ni SACs on CeO_2 support, the Ni–O_x catalytically active sites of which showed activity in the acetylene hydrogenation reaction at 200 °C. The achieved conversion was ~70%, and the calculated apparent activation energy coincided with the theoretical one of 0.53 eV, indicating that the C_2H_3* + H* = C_2H_4* reaction was the rate-determining step. However, the authors did not mention the selectivity values of the produced catalysts. Theoretical and practical studies of the Ni–N_x centers [128,147] have shown that the Ni–N_4 sites have a higher selectivity for ethylene in the acetylene hydrogenation reaction than the Ni–N_3 sites. For the latter, the selectivity dropped by 32% at 200 °C in 20 h of operation. This is due to the fact that the energy barrier for the desorption of the ethylene molecule turned out to be 1.5 times higher than that for ethane. Thus, by controlling the Ni coordination number, the catalyst could provide high ethylene selectivity.

4.2.3. Other Hydrogenation Reactions

In addition to the hydrogenation of carbon dioxide and acetylene, many other industrial processes rely on the efficient use of Ni catalysts in various hydrogenation reactions. For example, the reduction of organic compounds containing a nitro group to corresponding aniline derivatives is an important intermediate step in the pharmaceutical, agrochemical, pigmentation, and other industries. However, the use of catalysts containing Ni nanoparticles and prone to irreversible sintering or migration-coalescence hinders their long-term use. Currently, there are publications showing the efficient use of Ni SACs in the reduction of the nitro group in a hydrogen atmosphere [55,81]. In both reports, the Ni–N_3 sites showed high activity at a H_2 pressure of 3 MPa: Yang et al. [55] received 40.4% conversion in 1 h of reaction at 80 °C, while Zhou et al. [81] showed 99% conversion after 8 h of reaction at 120 °C. The calculated turnover frequencies (TOFs) were 37.6 and 8.4 h^{-1}, respectively. Interestingly, the Ni-N_4 site showed lower activity in the catalytic reaction. The authors of Ref. [55] attributed this to a partial polarization of the adsorbed hydrogen molecule and to a decrease in the co-adsorption energy of the next H_2 molecule, which facilitates the dissociation of hydrogen and its entry into the hydrogenation reaction. A similar effect was found by another group [81], where a higher reaction efficiency was associated with

the presence of a lower charge on the Ni atom, which led to a decrease in the energy barrier of H_2 dissociation as a result of electron donation from the Ni atom to the hydrogen molecule. However, regardless of a support used, all catalysts showed excellent selectivity (typically > 99%) for obtaining an amino group in the presence of various substituents in the organic molecule, such as –COOR, –COR, –OH, $–C_2H_3$, etc., in para-, ortho-, and meta-positions.

As mentioned above, the number of Ni atoms in the catalytically active site and the charge on them are important for activation of the H–H bond; however, the use of catalysts containing only Ni nanoparticles shows low efficiency. Ning et al. demonstrated the effect of Ni nanoparticles and Ni–N_x center synergy on the reaction of selective hydrogenation of cinnamaldehyde to phenylpropanal [148]. While separately, nanoparticles and Ni single-atoms showed a high conversion but a low selectivity, and vice versa, respectively, their combination in one catalyst made it possible to achieve 94.6% conversion and 83.7% selectivity to the desired product under the reaction conditions of 100 °C and 2 MPa of H_2 for 6 h flow. As the authors explained, this effect was achieved due to the activation of hydrogen molecules on Ni nanoparticles and their subsequent migration to the adsorbed and activated C=C bond of the cinnamaldehyde molecule on the Ni–N_x site with its subsequent reduction (Figure 11). Such a catalyst also turned out to be effective in the hydrogenation of other α, β–unsaturated aldehydes.

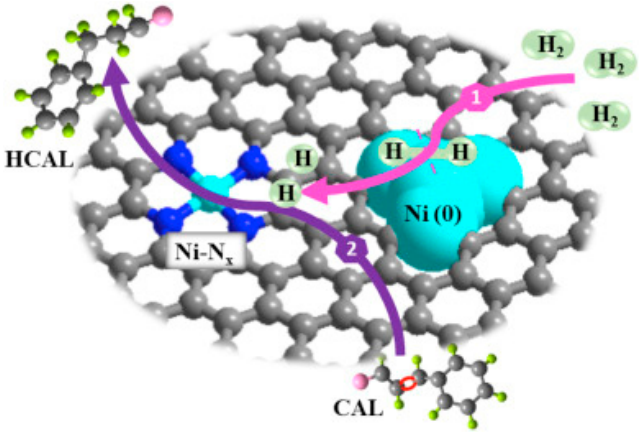

Figure 11. The proposed mechanism for selective hydrogenation of cinnamaldehyde to phenylpropanal is: (1) adsorption and activation of H_2 molecules on Ni^0 active sites; (2) adsorption and activation of cinnamaldehyde on Ni–N_x active sites. Reproduced with permission from [148]. Copyright 2019, Elsevier B.V.

4.3. O–H Activation

The use of hydrogen as a hydrogenating agent has some disadvantages associated with its gaseous state under ambient conditions. In the reactions discussed above, the typical hydrogen pressure was in the range of 1–3 MPa, which introduces difficulties in carrying out reactions both on laboratory and industrial scales. To overcome this, other molecules are used from which the hydrogen atom can be obtained, such as alcohols. Wang et al. studied the effect of the composition and structure of the Ni–N_xC_y site in graphene on the adsorption of isopropyl alcohol and the subsequent detachment of hydrogen from it [149]. The Ni–N_4 and Ni–N_3 sites turned out to be the most energetically favorable. It was shown that, despite the energetic preference for its formation, the flat structure of the Ni–N_4 site sterically prevents the dissociation of the O–H bond and makes the process highly endothermic. On the contrary, the Ni–N_3 site, in which the Ni atom protrudes above the graphene surface, not only easily adsorbs the isopropyl alcohol molecule due to the overlapping of the *p*-orbitals of the O atom and the *d*-orbitals of the Ni atom but also easily breaks the O–H bond.

4.3.1. Transfer Hydrogenation Reactions

Considering transfer hydrogenation reactions, in which alcohols act as donors of a hydrogen atom, one cannot fail to mention the Meerwein-Ponndorf-Verley (MPV) reduction reaction. This reaction involves the reduction of aldehydes and ketones to their corresponding alcohols, usually in the presence of aluminum alkoxide catalysts. A feature of this mechanism is the formation of a six-member ring transition state (Figure 12a, 2), which creates certain steric restrictions on the introduced reagents. The use of other catalysts, for example, Ni-based ones, can offset these limitations by changing the reaction mechanism to a radical one [79].

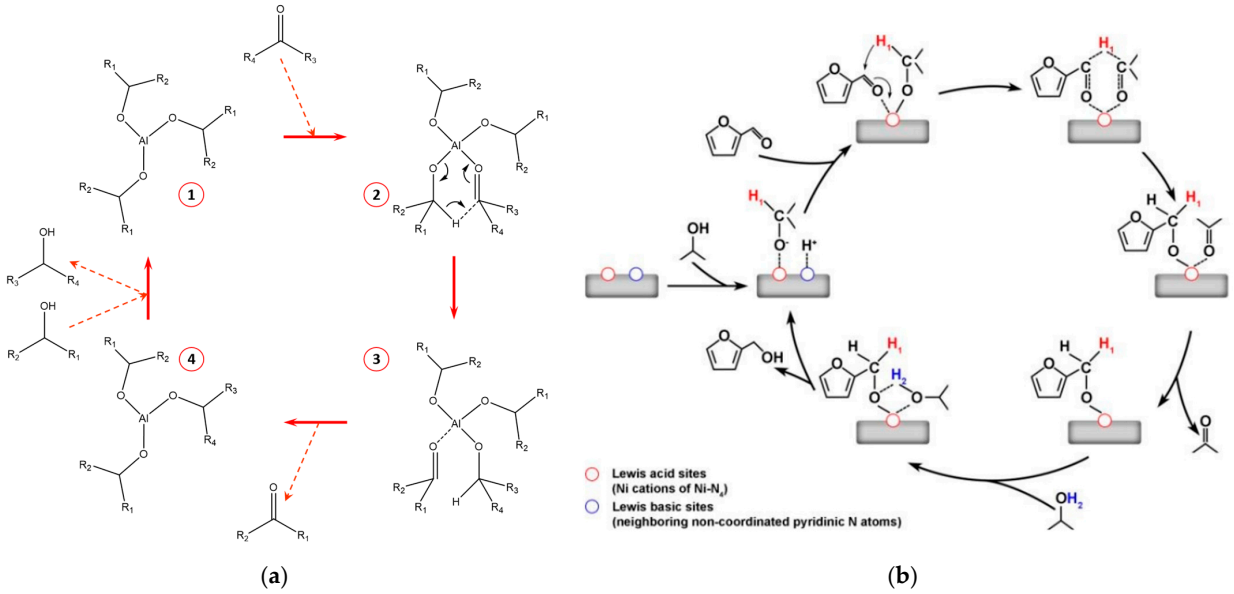

(**a**) (**b**)

Figure 12. (**a**) Catalytic cycle of the Meerwein-Ponndorf-Verley reduction reaction on an Al-based catalyst; (**b**) Possible mechanism for the catalytic transfer hydrogenation of furfural, reproduced with permission from [65]; Copyright 2021, The Royal Society of Chemistry.

Thus, using a Ni SAC, the hydrogen transfer reaction is initiated by the activation of the O–H bond of the hydrogen donor. In the theoretical work, Wang et al. considered two reaction mechanisms at the more active Ni–N_3 site [149]: with the initial dissociation of isopropyl alcohol into i–PrO* and H*, followed by the adsorption of furfural, or with the co-adsorption of both molecules. In the former case, the formation of a hydrogen atom was the energy-limiting stage of the process with a barrier energy of 0.83 eV, while in the latter case, there was a direct transfer of hydrogen from one molecule to another, overcoming the energy barrier of 1.32 eV. That is, carrying out the reaction on a catalytically active Ni atom made it possible both to lower the energy barrier of the reaction and to change its mechanism. The practically studied reduction reaction of 5–hydroxymethylfurfural with ethanol to 2,5–dihydroxymethylfuran on flat Ni–N_4 sites showed a radical mechanism of the reaction [79]. In this reaction, a conversion of 95% with almost 100% selectivity was achieved at a temperature of 160 °C, and the TOF of the reaction, 22 h^{-1}, was the highest reported in the literature. Consequently, the use of Ni SACs makes it possible not only to level the steric hindrances of the hydrogen transfer reaction but also to simplify it energetically.

It should be noted that there is another opinion in the literature concerning the reaction mechanism. Fan et al. studied the reaction of furfural reduction to furfuryl alcohol on Ni–N_4 sites using various alcohols as solvents and hydrogen donors: ethyl, propyl, 2–propyl, n–butyl, and 2–butyl alcohols [65]. According to the results, the reaction proceeded most efficiently in the presence of secondary alcohols with a smaller carbon chain, which clearly indicates the formation of the above mentioned six-membered transition state in

the reaction. The authors themselves proposed a possible mechanism for the reduction of furfural; however, the reaction was also initiated by the breaking of the O–H bond, and the resulting H* was directly involved in the reaction (Figure 12b).

Nickel has also been shown to be active in hydrogenation transfer coupling reactions, as reported by Zhang et al. for the conversion of nitrobenzene to azoxybenzene [89]. The authors succeeded in synthesizing Ni–N_4 and Ni–N_5 sites on a support of nitrogen-containing carbon spheres, which showed different efficiency in the reaction under study. At the reaction temperature of 50 °C for 3.5 h, the catalysts reached conversions of 99.2% and 95.6% vs. 38.8% and 33.1%, respectively, and the difference in calculated TOF was almost 2.5 times. The reason for this huge difference is the increased electron density on the nickel atom in the Ni–N_4 site, which contributes to the formation of H* species.

4.3.2. H_2 Production from Formic Acid

Formic acid is a widely used chemical in industry. It can be used as a safe, easy-to-handle, and transportable source of hydrogen for various reactions. The most widely accepted positive aspects of the synthesis and catalytic application of this acid can be found in the review by Bulushev and Ross [150]. Herein, we focus on its decomposition over Ni SACs. The HCOOH molecule is adsorbed on the nickel single atom, often via carbonyl oxygen. The gain in its adsorption energy is about 0.8 eV, which is an average value as compared with other transition metals and does not indicate too weak or too strong bonding with the metal atom [151]. In the literature devoted to the study of the mechanism of the HCOOH decomposition to H_2 and CO_2, there are two ways to initiate the reaction: through the formation of the formate species HCOO* (activation of the O–H bond) and through the formation of the carboxyl species *COOH (activation of the C–H bond). The second reaction route is less studied since the energy required to break the C–H bond in the formic acid molecule is usually much higher than that for the O–H bond [152,153]. Interestingly, some authors report a barrier-free pathway for the activation of the O–H bond [133,154].

Recall that the reaction of formic acid decomposition can proceed both in the gaseous and liquid phases. Gharib and Arab considered both approaches [151]. To approximate the liquid phase, the authors used the polarized continuum model for calculations. However, the reaction energies in the gas phase turned out to be lower than those in the liquid phase.

Depending on a chosen catalytic system and a calculation method, both the twisting motion of formate species with an activation energy of 0.9 eV [154] and the dissociation of HCOO* into CO_2* and H* with an activation energy of 0.87–1.06 eV are often considered to be the limiting stages of formic acid decomposition [133,152]. However, the reaction of recombination of adsorbed hydrogen atoms into the H_2 molecule also occurs [15,153]. The energy of this process is high and corresponds to 1.02–1.09 eV.

There is only one report in the literature in which the mechanism of formic acid decomposition in the gas phase over Ni SAC has been practically tested and theoretically calculated. We were able to apply 1 wt% Ni in the form of single atoms supported onto a porous carbon by simple impregnation [15]. The calculated mechanism of the reaction on the catalytically active Ni–N_4 sites showed the reaction proceeding through the formation of formate species. The rate-determining stage of the process was found to be the recombination of hydrogen atoms with an energy barrier of 1.09 eV (Figure 13a). In this work, the activity of Ni SAC was compared with the activity of Ni nanoparticles. At 300 °C, the conversion of formic acid over Ni–N_4 sites was 50% versus 30% obtained on Ni nanoparticles. The hydrogen selectivity for both catalysts was in the range of 95–97%. Recently, we have continued this research and increased the Ni content in catalysts up to 6 wt% [17]. The resulting catalysts showed close conversions of 46% and 58% for highly dispersed Ni and Ni nanoparticles, respectively, at the reaction temperature of 260 °C. Interestingly, despite the appearance of small Ni clusters, the formation of which occurred near the Ni–N_4 sites, the specific mass-based reaction rate of highly dispersed Ni catalysts remained unchanged, which indicates the equal activity of both forms of Ni in this reaction.

Rather, the reason could be that the reaction occurred at the Ni atom of the cluster and the closely located pyridinic N of the Ni-N_4 site (Figure 13b). It is noteworthy that the catalysts with Ni clusters were stable for 5 h at 250°C in the reaction conditions, while the catalysts with nanoparticles suffered deactivation.

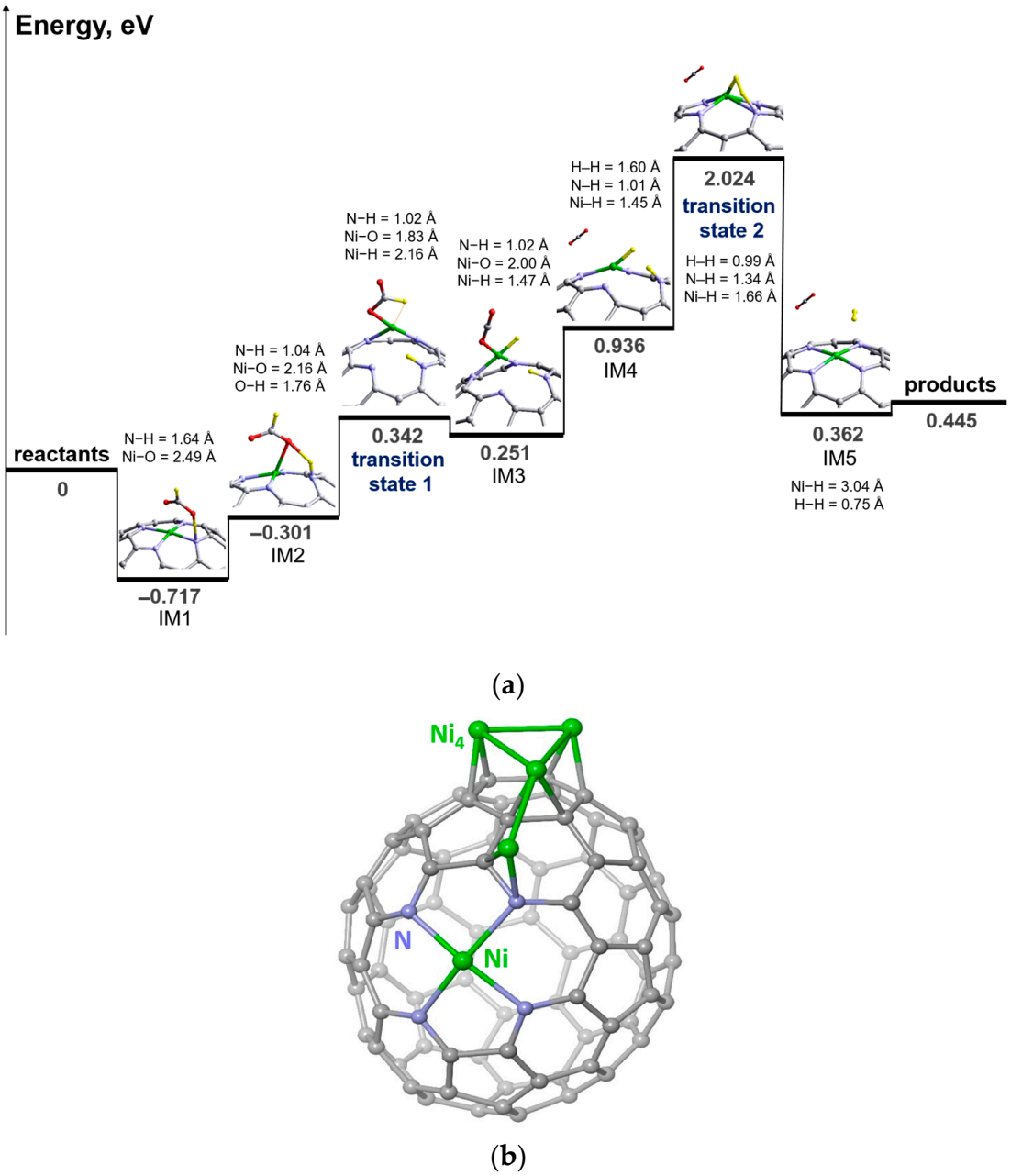

Figure 13. (**a**) Energy profile of the formic acid decomposition reaction over the Ni–N_4 site on the curved graphene. Reproduced with permission from [15], Copyright 2021, Elsevier B.V.; (**b**) Energetically preferable locations of four Ni atoms on the carbon cage with the Ni–N4 site. Adapted with permission from [17], Copyright 2023 by the Authors. Carbon, nitrogen, nickel, oxygen, and hydrogen atoms are represented by gray, violet, green, red, and yellow balls, respectively.

4.4. N–H Activation

In addition to the reactions of the formation of hydrogen atoms or molecules by activation of C–H, H–H, and O–H bonds, which are widely covered in the literature, some authors considered the possibility of using single-atom Ni sites for activation of other

bonds, for example, N–H. Feng et al. studied the mechanism of reduction of Br–C_6H_5–NO_2 to Br–C_6H_5–NH_2 at Ni–N_4 and Ni–N_3 sites using $N_2H_4 \cdot H_2O$ as a hydrogen donor [155]. Since the former catalytically active site exhibited significantly higher activity than the second one, the energy values given below correspond to the Ni–N_3 site. Hydrazine was adsorbed with the formation of the Ni–N bond, and the N–H bond breaking energy was equal to 0.93 eV, with both N_2H_3* and H* species remaining coordinated to the nickel atom. The subsequent adsorption of the R–NO_2 molecule was exothermic. The limiting stage of the reaction was the chemo-selective reduction process of the −NOH group through the recombination of the adsorbed hydrogen atom and the hydrogen atom of the −OH group—with an activation energy of 0.96 eV. The presence of the Br substituent did not adversely affect the reduction of the nitro group; moreover, the authors calculated that 1.18 eV would be required to break the C–Br bond, which makes this process kinetically unfavorable. In practice, the catalyst achieved 100% conversion and selectivity at 60 °C within 3 h of operation, and the calculated TOF was higher than that for the catalyst containing Ni nanoparticles.

It is interesting that theoretical calculations of the decomposition of N_2H_4 at the Ni–C_3 site did not show such good results as in the work [156]. The adsorption of the molecule on the catalytically active Ni atom still occurred due to the overlapping of the 3*d* and 2*p* orbitals of Ni and N, respectively. However, the authors calculated not only the dissociation of the N–H bond but also the dissociation of the N–N bond and showed that the second way is energetically preferable (0.86 and 0.51 eV, respectively). Moreover, the final state for the system after the N–H bond cleavage was endothermic, while after the N–N bond cleavage, it was exothermic, which indicates the potential unsuitability of the Ni–C_3 site as catalytically active in the production of H* from hydrazine. Although this site still showed potential activity and high selectivity in the formation of ammonia.

5. Summary

Known since the 19th century, Ni catalysts are widely used, even on an industrial scale. However, to reduce the cost of catalytic processes, it may be useful to switch to supported SACs. Thus, herein, we discuss the main approaches to the synthesis of Ni SACs and their application to break or form the X–H bond (where X = C, H, O, and N), thereby initializing the hydrogenation and dehydrogenation reactions.

The activity of Ni SACs in the C–H bond cleavage has been thoroughly studied for the DRM reaction. Supported Ni single atoms have been shown to be excellent for binding methane and its decomposition into CH_3* and H* species. The use of Ni SACs partially eliminates the Boudouard and complete cracking of methane reactions, and the further development of these catalysts is aimed precisely at the complete blocking of these side processes.

The cleavage of the H–H bond can proceed both homo- and heterolytically, which is strongly influenced by the atomic environment of the Ni center. Most often, the cleavage of this bond proceeds endothermically and is the limiting stage of the process. Despite the activity of Ni SACs in the hydrogenation of C_2H_2, CO_2, and various organic compounds, it may be more successful to use small clusters consisting of several Ni atoms.

The replacement of hydrogen by various alcohols or formic acid as hydrogen donors in hydrogenation reactions is associated with difficulties in working with H_2 under ambient conditions. This leads to another application of Ni SACs—their use in hydrogen transfer reactions. Due to the adsorbed hydrogen atom obtained on a Ni single atom as a result of the O–H dissociation, the reaction mechanism becomes radical, which eliminates possible steric hindrances. In addition, the breaking of the O–H bond becomes the limiting stage and, according to some DFT calculations, simplifies the reactions energetically. The high selectivity in hydrogenation reactions of various organic substituents makes Ni SACs indispensable in these types of reactions.

There are few examples of N–H bond cleavage in the literature. Using hydrazine as an example, it is shown that it is adsorbed on a Ni single atom and dissociates with

the abstraction of a hydrogen atom. However, breaking the N–N bond was even easier than breaking the H–H bond; therefore, the use of a Ni single atom to obtain H* or H_2 from hydrazine is energetically unfavorable. Over the past few years, no other sources of hydrogen have been used, and the potential of using Ni SACs has not been discovered.

One of the main disadvantages of metal-based SAC is the complexity of its preparation, especially when it comes to the high content (>5 wt%) of uniform single-atom sites. Despite numerous attempts to simplify and cheapen the catalyst synthesis while maintaining a high degree of metal loading, this has not yet been achieved. Thus, further development of Ni SACs is needed in the field of thermal catalysis, on which some industrial processes are based.

Author Contributions: Conceptualization, D.A.B. and A.D.N.; validation, D.A.B. and L.G.B.; writing—original draft preparation, A.D.N.; writing—review and editing, D.A.B. and L.G.B. All authors have read and agreed to the published version of the manuscript.

Funding: This work was supported by the Russian Science Foundation (grant No. 23-73-00048).

Data Availability Statement: Data is contained within the article.

Conflicts of Interest: The authors declare no conflict of interest.

References

1. Abundance in Earth's Crust for All the Elements in the Periodic Table. Available online: https://periodictable.com/Properties/A/CrustAbundance.html (accessed on 2 May 2023).
2. Sabatier, P. *Catalysis in Organic Chemistry*; D. Van Nostrand Company: New York, NY, USA, 1922.
3. Keim, W. Nickel: An Element with Wide Application in Industrial Homogeneous Catalysis. *Angew. Chem. Int. Ed. Engl.* **1990**, *29*, 235–244. [CrossRef]
4. Schneider, C.; Leischner, T.; Ryabchuk, P.; Jackstell, R.; Junge, K.; Beller, M. Development of Bulk Organic Chemical Processes—History, Status, and Opportunities for Academic Research. *CCS Chem.* **2021**, *3*, 512–530. [CrossRef]
5. Sun, Z.; Zhang, Z.-H.; Yuan, T.-Q.; Ren, X.; Rong, Z. Raney Ni as a Versatile Catalyst for Biomass Conversion. *ACS Catal.* **2021**, *11*, 10508–10536. [CrossRef]
6. Jette, E.R.; Foote, F. Precision Determination of Lattice Constants. *J. Chem. Phys.* **1935**, *3*, 605–616. [CrossRef]
7. Kaiser, S.K.; Chen, Z.; Faust Akl, D.; Mitchell, S.; Pérez-Ramírez, J. Single-Atom Catalysts across the Periodic Table. *Chem. Rev.* **2020**, *120*, 11703–11809. [CrossRef] [PubMed]
8. Shang, Y.; Duan, X.; Wang, S.; Yue, Q.; Gao, B.; Xu, X. Carbon-Based Single Atom Catalyst: Synthesis, Characterization, DFT Calculations. *Chin. Chem. Lett.* **2022**, *33*, 663–673. [CrossRef]
9. Qi, P.; Wang, J.; Djitcheu, X.; He, D.; Liu, H.; Zhang, Q. Techniques for the Characterization of Single Atom Catalysts. *RSC Adv.* **2022**, *12*, 1216–1227. [CrossRef] [PubMed]
10. Wu, J.; Xiong, L.; Zhao, B.; Liu, M.; Huang, L. Densely Populated Single Atom Catalysts. *Small Methods* **2020**, *4*, 1900540. [CrossRef]
11. Yang, J.; Li, W.; Wang, D.; Li, Y. Electronic Metal–Support Interaction of Single-Atom Catalysts and Applications in Electrocatalysis. *Adv. Mater.* **2020**, *32*, 2003300. [CrossRef]
12. Qi, K.; Chhowalla, M.; Voiry, D. Single Atom Is Not Alone: Metal–Support Interactions in Single-Atom Catalysis. *Mater. Today* **2020**, *40*, 173–192. [CrossRef]
13. Kottwitz, M.; Li, Y.; Wang, H.; Frenkel, A.I.; Nuzzo, R.G. Single Atom Catalysts: A Review of Characterization Methods. *Chemistry–Methods* **2021**, *1*, 278–294. [CrossRef]
14. Liu, J.; Bunes, B.R.; Zang, L.; Wang, C. Supported Single-Atom Catalysts: Synthesis, Characterization, Properties, and Applications. *Environ. Chem. Lett.* **2018**, *16*, 477–505. [CrossRef]
15. Bulushev, D.A.; Nishchakova, A.D.; Trubina, S.V.; Stonkus, O.A.; Asanov, I.P.; Okotrub, A.V.; Bulusheva, L.G. Ni-N_4 Sites in a Single-Atom Ni Catalyst on N-Doped Carbon for Hydrogen Production from Formic Acid. *J. Catal.* **2021**, *402*, 264–274. [CrossRef]
16. Yang, H.; Lin, Q.; Zhang, C.; Yu, X.; Cheng, Z.; Li, G.; Hu, Q.; Ren, X.; Zhang, Q.; Liu, J.; et al. Carbon Dioxide Electroreduction on Single-Atom Nickel Decorated Carbon Membranes with Industry Compatible Current Densities. *Nat. Commun.* **2020**, *11*, 593. [CrossRef]
17. Nishchakova, A.D.; Bulushev, D.A.; Trubina, S.V.; Stonkus, O.A.; Shubin, Y.V.; Asanov, I.P.; Kriventsov, V.V.; Okotrub, A.V.; Bulusheva, L.G. Highly Dispersed Ni on Nitrogen-Doped Carbon for Stable and Selective Hydrogen Generation from Gaseous Formic Acid. *Nanomaterials* **2023**, *13*, 545. [CrossRef]
18. Li, Y.; Wu, Z.; Lu, P.; Wang, X.; Liu, W.; Liu, Z.; Ma, J.; Ren, W.; Jiang, Z.; Bao, X. High-Valence Nickel Single-Atom Catalysts Coordinated to Oxygen Sites for Extraordinarily Activating Oxygen Evolution Reaction. *Adv. Sci.* **2020**, *7*, 1903089. [CrossRef]

19. Li, Y.; Lu, X.F.; Xi, S.; Luan, D.; Wang, X.; Lou, X.W. (David) Synthesis of N-Doped Highly Graphitic Carbon Urchin-Like Hollow Structures Loaded with Single-Ni Atoms towards Efficient CO_2 Electroreduction. *Angew. Chem. Int. Ed.* **2022**, *61*, e202201491. [CrossRef]
20. Wang, Y.; Shi, R.; Shang, L.; Waterhouse, G.I.N.; Zhao, J.; Zhang, Q.; Gu, L.; Zhang, T. High-Efficiency Oxygen Reduction to Hydrogen Peroxide Catalyzed by Nickel Single-Atom Catalysts with Tetradentate N_2O_2 Coordination in a Three-Phase Flow Cell. *Angew. Chem. Int. Ed.* **2020**, *59*, 13057–13062. [CrossRef]
21. Büchele, S.; Martín, A.J.; Mitchell, S.; Krumeich, F.; Collins, S.M.; Xi, S.; Borgna, A.; Pérez-Ramírez, J. Structure Sensitivity and Evolution of Nickel-Bearing Nitrogen-Doped Carbons in the Electrochemical Reduction of CO_2. *ACS Catal.* **2020**, *10*, 3444–3454. [CrossRef]
22. Yang, H.; Shang, L.; Zhang, Q.; Shi, R.; Waterhouse, G.I.N.; Gu, L.; Zhang, T. A Universal Ligand Mediated Method for Large Scale Synthesis of Transition Metal Single Atom Catalysts. *Nat. Commun.* **2019**, *10*, 4585. [CrossRef]
23. Mou, K.; Chen, Z.; Zhang, X.; Jiao, M.; Zhang, X.; Ge, X.; Zhang, W.; Liu, L. Highly Efficient Electroreduction of CO_2 on Nickel Single-Atom Catalysts: Atom Trapping and Nitrogen Anchoring. *Small* **2019**, *15*, 1903668. [CrossRef]
24. Liu, W.; Chen, Y.; Qi, H.; Zhang, L.; Yan, W.; Liu, X.; Yang, X.; Miao, S.; Wang, W.; Liu, C.; et al. A Durable Nickel Single-Atom Catalyst for Hydrogenation Reactions and Cellulose Valorization under Harsh Conditions. *Angew. Chem. Int. Ed.* **2018**, *57*, 7071–7075. [CrossRef]
25. Wei, S.; Wang, Y.; Chen, W.; Li, Z.; Cheong, W.-C.; Zhang, Q.; Gong, Y.; Gu, L.; Chen, C.; Wang, D.; et al. Atomically Dispersed Fe Atoms Anchored on COF-Derived N-Doped Carbon Nanospheres as Efficient Multi-Functional Catalysts. *Chem. Sci.* **2019**, *11*, 786–790. [CrossRef]
26. Ochoa-Gómez, J.R.; Roncal, T. Production of Sorbitol from Biomass. In *Production of Platform Chemicals from Sustainable Resources*; Biofuels and, Biorefineries; Fang, Z., Smith, R.L., Qi, X., Eds.; Springer: Singapore, 2017; pp. 265–309. ISBN 978-981-10-4171-6.
27. Zhu, L.; Sun, H.; Fu, H.; Zheng, J.; Zhang, N.; Li, Y.; Chen, B.H. Effect of Ruthenium Nickel Bimetallic Composition on the Catalytic Performance for Benzene Hydrogenation to Cyclohexane. *Appl. Catal. Gen.* **2015**, *499*, 124–132. [CrossRef]
28. Copéret, C.; Allouche, F.; Chan, K.W.; Conley, M.P.; Delley, M.F.; Fedorov, A.; Moroz, I.B.; Mougel, V.; Pucino, M.; Searles, K.; et al. Bridging the Gap between Industrial and Well-Defined Supported Catalysts. *Angew. Chem. Int. Ed.* **2018**, *57*, 6398–6440. [CrossRef]
29. Finiels, A.; Fajula, F.; Hulea, V. Nickel-Based Solid Catalysts for Ethylene Oligomerization—A Review. *Catal. Sci. Technol.* **2014**, *4*, 2412–2426. [CrossRef]
30. LaMer, V.K.; Dinegar, R.H. Theory, Production and Mechanism of Formation of Monodispersed Hydrosols. *J. Am. Chem. Soc.* **1950**, *72*, 4847–4854. [CrossRef]
31. Lepre, E.; Heske, J.; Nowakowski, M.; Scoppola, E.; Zizak, I.; Heil, T.; Kühne, T.D.; Antonietti, M.; López-Salas, N.; Albero, J. Ni-Based Electrocatalysts for Unconventional CO_2 Reduction Reaction to Formic Acid. *Nano Energy* **2022**, *97*, 107191. [CrossRef]
32. Wang, Q.; Zhao, Z.L.; Dong, S.; He, D.; Lawrence, M.J.; Han, S.; Cai, C.; Xiang, S.; Rodriguez, P.; Xiang, B.; et al. Design of Active Nickel Single-Atom Decorated MoS_2 as a PH-Universal Catalyst for Hydrogen Evolution Reaction. *Nano Energy* **2018**, *53*, 458–467. [CrossRef]
33. Rong, X.; Wang, H.; Lu, X.; Si, R.; Lu, T. Controlled Synthesis of a Vacancy-Defect Single-Atom Catalyst for Boosting CO_2 Electroreduction. *Angew. Chem. Int. Ed.* **2019**, *59*, 1961–1965. [CrossRef]
34. Yan, C.; Li, H.; Ye, Y.; Wu, H.; Cai, F.; Si, R.; Xiao, J.; Miao, S.; Xie, S.; Yang, F.; et al. Coordinatively Unsaturated Nickel–Nitrogen Sites towards Selective and High-Rate CO_2 Electroreduction. *Energy Environ. Sci.* **2018**, *11*, 1204–1210. [CrossRef]
35. Wu, S.; Yi, F.; Ping, D.; Huang, S.; Zhang, Y.; Han, L.; Wang, S.; Wang, H.; Yang, X.; Guo, D.; et al. Constructing Single-Atomic Nickel Sites in Carbon Nanotubes for Efficient CO_2 Electroreduction. *Carbon* **2022**, *196*, 1–9. [CrossRef]
36. Cheng, Y.; Zhao, S.; Johannessen, B.; Veder, J.; Saunders, M.; Rowles, M.R.; Cheng, M.; Liu, C.; Chisholm, M.F.; Marco, R.; et al. Atomically Dispersed Transition Metals on Carbon Nanotubes with Ultrahigh Loading for Selective Electrochemical Carbon Dioxide Reduction. *Adv. Mater.* **2018**, *30*, 1706287. [CrossRef]
37. Fei, H.; Dong, J.; Feng, Y.; Allen, C.S.; Wan, C.; Volosskiy, B.; Li, M.; Zhao, Z.; Wang, Y.; Sun, H.; et al. General Synthesis and Definitive Structural Identification of MN_4C_4 Single-Atom Catalysts with Tunable Electrocatalytic Activities. *Nat. Catal.* **2018**, *1*, 63–72. [CrossRef]
38. Jeong, H.; Balamurugan, M.; Choutipalli, V.S.K.; Jo, J.; Baik, H.; Subramanian, V.; Kim, M.; Sim, U.; Nam, K.T. Tris(2-benzimidazolylmethyl)Amine-Directed Synthesis of Single-Atom Nickel Catalysts for Electrochemical CO Production from CO_2. *Chem. Eur. J.* **2018**, *24*, 18444–18454. [CrossRef]
39. Bi, W.; Li, X.; You, R.; Chen, M.; Yuan, R.; Huang, W.; Wu, X.; Chu, W.; Wu, C.; Xie, Y. Surface Immobilization of Transition Metal Ions on Nitrogen-Doped Graphene Realizing High-Efficient and Selective CO_2 Reduction. *Adv. Mater.* **2018**, *30*, 1706617. [CrossRef]
40. Pan, F.; Deng, W.; Justiniano, C.; Li, Y. Identification of Champion Transition Metals Centers in Metal and Nitrogen-Codoped Carbon Catalysts for CO_2 Reduction. *Appl. Catal. B Environ.* **2018**, *226*, 463–472. [CrossRef]
41. Yang, H.B.; Hung, S.-F.; Liu, S.; Yuan, K.; Miao, S.; Zhang, L.; Huang, X.; Wang, H.-Y.; Cai, W.; Chen, R.; et al. Atomically Dispersed Ni(i) as the Active Site for Electrochemical CO_2 Reduction. *Nat. Energy* **2018**, *3*, 140–147. [CrossRef]

42. Su, H.; Gao, P.; Wang, M.; Zhai, G.; Zhang, J.; Zhao, T.; Su, J.; Antonietti, M.; Li, X.; Chen, J. Grouping Effect of Single Nickel−N_4 Sites in Nitrogen-Doped Carbon Boosts Hydrogen Transfer Coupling of Alcohols and Amines. *Angew. Chem. Int. Ed.* **2018**, *57*, 15194–15198. [CrossRef]
43. Zhao, S.; Cheng, Y.; Veder, J.-P.; Johannessen, B.; Saunders, M.; Zhang, L.; Liu, C.; Chisholm, M.F.; De Marco, R.; Liu, J.; et al. One-Pot Pyrolysis Method to Fabricate Carbon Nanotube Supported Ni Single-Atom Catalysts with Ultrahigh Loading. *ACS Appl. Energy Mater.* **2018**, *10*, 5286–5297. [CrossRef]
44. Zhu, Y.; Sun, W.; Luo, J.; Chen, W.; Cao, T.; Zheng, L.; Dong, J.; Zhang, J.; Zhang, M.; Han, Y.; et al. A Cocoon Silk Chemistry Strategy to Ultrathin N-Doped Carbon Nanosheet with Metal Single-Site Catalysts. *Nat. Commun.* **2018**, *9*, 3861. [CrossRef] [PubMed]
45. Fei, H.; Dong, J.; Wan, C.; Zhao, Z.; Xu, X.; Lin, Z.; Wang, Y.; Liu, H.; Zang, K.; Luo, J.; et al. Microwave-Assisted Rapid Synthesis of Graphene-Supported Single Atomic Metals. *Adv. Mater.* **2018**, *30*, 1802146. [CrossRef]
46. Yang, J.; Qiu, Z.; Zhao, C.; Wei, W.; Chen, W.; Li, Z.; Qu, Y.; Dong, J.; Luo, J.; Li, Z.; et al. In Situ Thermal Atomization to Convert Supported Nickel Nanoparticles into Surface-Bound Nickel Single-Atom Catalysts. *Angew. Chem. Int. Ed.* **2018**, *57*, 14095–14100. [CrossRef] [PubMed]
47. Xue, Y.; Huang, B.; Yi, Y.; Guo, Y.; Zuo, Z.; Li, Y.; Jia, Z.; Liu, H.; Li, Y. Anchoring Zero Valence Single Atoms of Nickel and Iron on Graphdiyne for Hydrogen Evolution. *Nat. Commun.* **2018**, *9*, 1460. [CrossRef] [PubMed]
48. Zhang, L.; Jia, Y.; Gao, G.; Yan, X.; Chen, N.; Chen, J.; Soo, M.T.; Wood, B.; Yang, D.; Du, A.; et al. Graphene Defects Trap Atomic Ni Species for Hydrogen and Oxygen Evolution Reactions. *Chem* **2018**, *4*, 285–297. [CrossRef]
49. Zhang, H.; Yu, L.; Chen, T.; Zhou, W.; Lou, X.W.D. Surface Modulation of Hierarchical MoS_2 Nanosheets by Ni Single Atoms for Enhanced Electrocatalytic Hydrogen Evolution. *Adv. Funct. Mater.* **2018**, *28*, 1807086. [CrossRef]
50. Fan, Q.; Hou, P.; Choi, C.; Wu, T.; Hong, S.; Li, F.; Soo, Y.; Kang, P.; Jung, Y.; Sun, Z. Activation of Ni Particles into Single Ni–N Atoms for Efficient Electrochemical Reduction of CO_2. *Adv. Energy Mater.* **2019**, *10*, 1903068. [CrossRef]
51. Hou, Y.; Qiu, M.; Kim, M.G.; Liu, P.; Nam, G.; Zhang, T.; Zhuang, X.; Yang, B.; Cho, J.; Chen, M.; et al. Atomically Dispersed Nickel–Nitrogen–Sulfur Species Anchored on Porous Carbon Nanosheets for Efficient Water Oxidation. *Nat. Commun.* **2019**, *10*, 1392. [CrossRef]
52. Wu, Y.; Jiang, Z.; Lu, X.; Liang, Y.; Wang, H. Domino Electroreduction of CO_2 to Methanol on a Molecular Catalyst. *Nature* **2019**, *575*, 639–642. [CrossRef]
53. Zhang, H.; Liu, Y.; Chen, T.; Zhang, J.; Zhang, J.; Lou, X.W. (David) Unveiling the Activity Origin of Electrocatalytic Oxygen Evolution over Isolated Ni Atoms Supported on a N-Doped Carbon Matrix. *Adv. Mater.* **2019**, *31*, 1904548. [CrossRef]
54. Lu, C.; Yang, J.; Wei, S.; Bi, S.; Xia, Y.; Chen, M.; Hou, Y.; Qiu, M.; Yuan, C.; Su, Y.; et al. Atomic Ni Anchored Covalent Triazine Framework as High Efficient Electrocatalyst for Carbon Dioxide Conversion. *Adv. Funct. Mater.* **2019**, *29*, 1806884. [CrossRef]
55. Yang, F.; Wang, M.; Liu, W.; Yang, B.; Wang, Y.; Luo, J.; Tang, Y.; Hou, L.; Li, Y.; Li, Z.; et al. Atomically Dispersed Ni as the Active Site towards Selective Hydrogenation of Nitroarenes. *Green Chem.* **2019**, *21*, 704–711. [CrossRef]
56. Lu, P.; Yang, Y.; Yao, J.; Wang, M.; Dipazir, S.; Yuan, M.; Zhang, J.; Wang, X.; Xie, Z.; Zhang, G. Facile Synthesis of Single-Nickel-Atomic Dispersed N-Doped Carbon Framework for Efficient Electrochemical CO_2 Reduction. *Appl. Catal. B Environ.* **2019**, *241*, 113–119. [CrossRef]
57. Zhang, L.; Liu, D.; Muhammad, Z.; Wan, F.; Xie, W.; Wang, Y.; Song, L.; Niu, Z.; Chen, J. Single Nickel Atoms on Nitrogen-Doped Graphene Enabling Enhanced Kinetics of Lithium–Sulfur Batteries. *Adv. Mater.* **2019**, *31*, 1903955. [CrossRef]
58. Jeong, H.-Y.; Balamurugan, M.; Choutipalli, V.S.K.; Jeong, E.; Subramanian, V.; Sim, U.; Nam, K.T. Achieving Highly Efficient CO_2 to CO Electroreduction Exceeding 300 MA Cm^{-2} with Single-Atom Nickel Electrocatalysts. *J. Mater. Chem. A* **2019**, *7*, 10651–10661. [CrossRef]
59. Tang, Y.; Wei, Y.; Wang, Z.; Zhang, S.; Li, Y.; Nguyen, L.; Li, Y.; Zhou, Y.; Shen, W.; Tao, F.F.; et al. Synergy of Single-Atom Ni_1 and Ru_1 Sites on CeO_2 for Dry Reforming of CH_4. *J. Am. Chem. Soc.* **2019**, *141*, 7283–7293. [CrossRef]
60. Akri, M.; Zhao, S.; Li, X.; Zang, K.; Lee, A.F.; Isaacs, M.A.; Xi, W.; Gangarajula, Y.; Luo, J.; Ren, Y.; et al. Atomically Dispersed Nickel as Coke-Resistant Active Sites for Methane Dry Reforming. *Nat. Commun.* **2019**, *10*, 5181. [CrossRef]
61. Li, Y.; Hao, J.; Song, H.; Zhang, F.; Bai, X.; Meng, X.; Zhang, H.; Wang, S.; Hu, Y.; Ye, J. Selective Light Absorber-Assisted Single Nickel Atom Catalysts for Ambient Sunlight-Driven CO_2 Methanation. *Nat. Commun.* **2019**, *10*, 2359. [CrossRef]
62. Xiong, W.; Li, H.; Wang, H.; Yi, J.; You, H.; Zhang, S.; Hou, Y.; Cao, M.; Zhang, T.; Cao, R. Hollow Mesoporous Carbon Sphere Loaded Ni–N_4 Single-Atom: Support Structure Study for CO_2 Electrocatalytic Reduction Catalyst. *Small* **2020**, *16*, 2003943. [CrossRef]
63. Yang, X.; Cheng, J.; Fang, B.; Xuan, X.; Liu, N.; Yang, X.; Zhou, J. Single Ni Atoms with Higher Positive Charges Induced by Hydroxyls for Electrocatalytic CO_2 Reduction. *Nanoscale* **2020**, *12*, 18437–18445. [CrossRef]
64. Zhou, M.; Jiang, Y.; Wang, G.; Wu, W.; Chen, W.; Yu, P.; Lin, Y.; Mao, J.; Mao, L. Single-Atom Ni-N_4 Provides a Robust Cellular NO Sensor. *Nat. Commun.* **2020**, *11*, 3188. [CrossRef] [PubMed]
65. Fan, Y.; Zhuang, C.; Li, S.; Wang, Y.; Zou, X.; Liu, X.; Huang, W.; Zhu, G. Efficient Single-Atom Ni for Catalytic Transfer Hydrogenation of Furfural to Furfuryl Alcohol. *J. Mater. Chem. A* **2020**, *9*, 1110–1118. [CrossRef]
66. Sa, Y.J.; Jung, H.; Shin, D.; Jeong, H.Y.; Ringe, S.; Kim, H.; Hwang, Y.J.; Joo, S.H. Thermal Transformation of Molecular Ni^{2+}–N_4 Sites for Enhanced CO_2 Electroreduction Activity. *ACS Catal.* **2020**, *10*, 10920–10931. [CrossRef]

67. Liu, S.; Yang, H.B.; Hung, S.; Ding, J.; Cai, W.; Liu, L.; Gao, J.; Li, X.; Ren, X.; Kuang, Z.; et al. Elucidating the Electrocatalytic CO_2 Reduction Reaction over a Model Single-Atom Nickel Catalyst. *Angew. Chem. Int. Ed.* **2020**, *59*, 798–803. [CrossRef] [PubMed]
68. Koshy, D.M.; Chen, S.; Lee, D.U.; Stevens, M.B.; Abdellah, A.M.; Dull, S.M.; Chen, G.; Nordlund, D.; Gallo, A.; Hahn, C.; et al. Understanding the Origin of Highly Selective CO_2 Electroreduction to CO on Ni,N-doped Carbon Catalysts. *Angew. Chem. Int. Ed.* **2020**, *59*, 4043–4050. [CrossRef] [PubMed]
69. Zhang, X.; Wang, Y.; Gu, M.; Wang, M.; Zhang, Z.; Pan, W.; Jiang, Z.; Zheng, H.; Lucero, M.; Wang, H.; et al. Molecular Engineering of Dispersed Nickel Phthalocyanines on Carbon Nanotubes for Selective CO_2 Reduction. *Nat. Energy* **2020**, *5*, 684–692. [CrossRef]
70. Gong, Y.; Jiao, L.; Qian, Y.; Pan, C.; Zheng, L.; Cai, X.; Liu, B.; Yu, S.; Jiang, H. Regulating the Coordination Environment of MOF-Templated Single-Atom Nickel Electrocatalysts for Boosting CO_2 Reduction. *Angew. Chem. Int. Ed.* **2020**, *59*, 2705–2709. [CrossRef]
71. Li, S.; Ceccato, M.; Lu, X.; Frank, S.; Lock, N.; Roldan, A.; Hu, X.-M.; Skrydstrup, T.; Daasbjerg, K. Incorporation of Nickel Single Atoms into Carbon Paper as Self-Standing Electrocatalyst for CO_2 Reduction. *J. Mater. Chem. A* **2020**, *9*, 1583–1592. [CrossRef]
72. Zhang, C.; Fu, Z.; Zhao, Q.; Du, Z.; Zhang, R.; Li, S. Single-Atom-Ni-Decorated, Nitrogen-Doped Carbon Layers for Efficient Electrocatalytic CO_2 Reduction Reaction. *Electrochem. Commun.* **2020**, *116*, 106758. [CrossRef]
73. Chen, J.; Li, H.; Fan, C.; Meng, Q.; Tang, Y.; Qiu, X.; Fu, G.; Ma, T. Dual Single-Atomic Ni-N_4 and Fe-N_4 Sites Constructing Janus Hollow Graphene for Selective Oxygen Electrocatalysis. *Adv. Mater.* **2020**, *32*, 2003134. [CrossRef]
74. Cai, Z.; Du, P.; Liang, W.; Zhang, H.; Wu, P.; Cai, C.; Yan, Z. Single-Atom-Sized Ni–N $_4$ Sites Anchored in Three-Dimensional Hierarchical Carbon Nanostructures for the Oxygen Reduction Reaction. *J. Mater. Chem. A* **2020**, *8*, 15012–15022. [CrossRef]
75. Luo, F.; Zhu, J.; Ma, S.; Li, M.; Xu, R.; Zhang, Q.; Yang, Z.; Qu, K.; Cai, W.; Chen, Z. Regulated Coordination Environment of Ni Single Atom Catalyst toward High-Efficiency Oxygen Electrocatalysis for Rechargeable Zinc-Air Batteries. *Energy Storage Mater.* **2021**, *35*, 723–730. [CrossRef]
76. Zhao, X.; Huang, S.; Chen, Z.; Lu, C.; Han, S.; Ke, C.; Zhu, J.; Zhang, J.; Tranca, D.; Zhuang, X. Carbon Nanosheets Supporting Ni–N_3S Single-Atom Sites for Efficient Electrocatalytic CO_2 Reduction. *Carbon* **2021**, *178*, 488–496. [CrossRef]
77. Zhang, S.; Ao, X.; Huang, J.; Wei, B.; Zhai, Y.; Zhai, D.; Deng, W.; Su, C.; Wang, D.; Li, Y. Isolated Single-Atom Ni–N_5 Catalytic Site in Hollow Porous Carbon Capsules for Efficient Lithium–Sulfur Batteries. *Nano Lett.* **2021**, *21*, 9691–9698. [CrossRef]
78. Zhang, Y.; Jiao, L.; Yang, W.; Xie, C.; Jiang, H. Rational Fabrication of Low-Coordinate Single-Atom Ni Electrocatalysts by MOFs for Highly Selective CO_2 Reduction. *Angew. Chem. Int. Ed.* **2021**, *60*, 7607–7611. [CrossRef]
79. Feng, Y.; Long, S.; Chen, B.; Jia, W.; Xie, S.; Sun, Y.; Tang, X.; Yang, S.; Zeng, X.; Lin, L. Inducing Electron Dissipation of Pyridinic N Enabled by Single Ni–N_4 Sites for the Reduction of Aldehydes/Ketones with Ethanol. *ACS Catal.* **2021**, *11*, 6398–6405. [CrossRef]
80. Jia, C.; Li, S.; Zhao, Y.; Hocking, R.K.; Ren, W.; Chen, X.; Su, Z.; Yang, W.; Wang, Y.; Zheng, S.; et al. Nitrogen Vacancy Induced Coordinative Reconstruction of Single-Atom Ni Catalyst for Efficient Electrochemical CO_2 Reduction. *Adv. Funct. Mater.* **2021**, *31*, 2107072. [CrossRef]
81. Zhou, D.; Zhang, L.; Liu, X.; Qi, H.; Liu, Q.; Yang, J.; Su, Y.; Ma, J.; Yin, J.; Wang, A. Tuning the Coordination Environment of Single-Atom Catalyst M-N-C towards Selective Hydrogenation of Functionalized Nitroarenes. *Nano Res.* **2021**, *15*, 519–527. [CrossRef]
82. Svalova, A.; Brusko, V.; Sultanova, E.; Kirsanova, M.; Khamidullin, T.; Vakhitov, I.; Dimiev, A.M. Individual Ni Atoms on Reduced Graphene Oxide as Efficient Catalytic System for Reduction of 4-Nitrophenol. *Appl. Surf. Sci.* **2021**, *565*, 150503. [CrossRef]
83. Mei, B.; Liu, C.; Sun, F.; Lu, S.; Du, X.; Li, X.; Song, F.; Xu, W.; Jiang, Z. Unraveling the Potential-Dependent Volcanic Selectivity Changes of an Atomically Dispersed Ni Catalyst During CO_2 Reduction. *ACS Catal.* **2022**, *12*, 8676–8686. [CrossRef]
84. Li, Y.; Adli, N.M.; Shan, W.; Wang, M.; Zachman, M.J.; Hwang, S.; Tabassum, H.; Karakalos, S.; Feng, Z.; Wang, G.; et al. Atomically Dispersed Single Ni Site Catalysts for High-Efficiency CO_2 Electroreduction at Industrial-Level Current Densities. *Energy Environ. Sci.* **2022**, *15*, 2108–2119. [CrossRef]
85. Zhu, J.; Wang, X.; Ke, T.; Jia, M.; Jin, B.; Li, Y.; Yang, Q.; Ren, L.; Ren, Y.; Cheng, D.; et al. Nickel Single Atom Overcoordinated Active Sites to Accelerate the Electrochemical Reaction Kinetics for Li-S Cathode. *J. Energy Chem.* **2022**, *78*, 203–210. [CrossRef]
86. Chen, K.; Cao, M.; Lin, Y.; Fu, J.; Liao, H.; Zhou, Y.; Li, H.; Qiu, X.; Hu, J.; Zheng, X.; et al. Ligand Engineering in Nickel Phthalocyanine to Boost the Electrocatalytic Reduction of CO_2. *Adv. Funct. Mater.* **2022**, *32*, 2111322. [CrossRef]
87. Huang, M.; Deng, B.; Zhao, X.; Zhang, Z.; Li, F.; Li, K.; Cui, Z.; Kong, L.; Lu, J.; Dong, F.; et al. Template-Sacrificing Synthesis of Well-Defined Asymmetrically Coordinated Single-Atom Catalysts for Highly Efficient CO_2 Electrocatalytic Reduction. *ACS Nano* **2022**, *16*, 2110–2119. [CrossRef] [PubMed]
88. Xi, D.; Li, J.; Low, J.; Mao, K.; Long, R.; Li, J.; Dai, Z.; Shao, T.; Zhong, Y.; Li, Y.; et al. Limiting the Uncoordinated N Species in M–N_x Single-Atom Catalysts toward Electrocatalytic CO_2 Reduction in Broad Voltage Range. *Adv. Mater.* **2022**, *34*, 2104090. [CrossRef] [PubMed]
89. Zhang, T.; Xie, Z.; Jiang, L.; Zhao, W.; Cao, S.; Wang, B.; Si, R.; Zhang, R.; Liu, Y.; Zhao, Z. Selective Transfer Hydrogenation Coupling of Nitroaromatics to Azoxy/Azo Compounds by Electron-Enriched Single Ni-N_4 Sites on Mesoporous N-Doped Carbon. *Chem. Eng. J.* **2022**, *443*, 136416. [CrossRef]
90. Li, Y.; Zhang, S.L.; Cheng, W.; Chen, Y.; Luan, D.; Gao, S.; Lou, X.W. (David) Loading Single-Ni Atoms on Assembled Hollow N-Rich Carbon Plates for Efficient CO_2 Electroreduction. *Adv. Mater.* **2022**, *34*, 2105204. [CrossRef] [PubMed]
91. Li, Y.; Zeng, Y.; Chen, Y.; Luan, D.; Gao, S.; Lou, X.W. (David) Mesoporous N-rich Carbon with Single-Ni Atoms as a Multifunctional Sulfur Host for Li-S Batteries. *Angew. Chem. Int. Ed.* **2022**, *61*, e202212680. [CrossRef]

92. Huang, J.; Qiu, X.; Zhao, Z.; Zhu, H.; Liu, Y.; Shi, W.; Liao, P.; Chen, X. Single-Product Faradaic Efficiency for Electrocatalytic of CO_2 to CO at Current Density Larger than 1.2 A Cm^{-2} in Neutral Aqueous Solution by a Single-Atom Nanozyme. *Angew. Chem. Int. Ed.* **2022**, *61*, e202210985. [CrossRef]
93. Yang, X.; Cheng, J.; Lv, H.; Yang, X.; Ding, L.; Xu, Y.; Zhang, K.; Sun, W.; Zhou, J. Sulfur-Doped Unsaturated Ni-N_3 Coordination for Efficient Electroreduction of CO_2. *Chem. Eng. J.* **2022**, *450*, 137950. [CrossRef]
94. Leverett, J.; Yuwono, J.A.; Kumar, P.; Tran-Phu, T.; Qu, J.; Cairney, J.; Wang, X.; Simonov, A.N.; Hocking, R.K.; Johannessen, B.; et al. Impurity Tolerance of Unsaturated Ni-N-C Active Sites for Practical Electrochemical CO_2 Reduction. *ACS Energy Lett.* **2022**, *7*, 920–928. [CrossRef]
95. Liu, X.; Liao, L.; Xia, G.; Yu, F.; Zhang, G.; Shu, M.; Wang, H. An Accurate "Metal Pre-Buried" Strategy for Constructing Ni–N_2C_2 Single-Atom Sites with High Metal Loadings toward Electrocatalytic CO_2 Reduction. *J. Mater. Chem. A* **2022**, *10*, 25047–25054. [CrossRef]
96. Zhao, Y.; Lu, X.F.; Fan, G.; Luan, D.; Gu, X.; Lou, X.W. (David) Surface-Exposed Single-Ni Atoms with Potential-Driven Dynamic Behaviors for Highly Efficient Electrocatalytic Oxygen Evolution. *Angew. Chem. Int. Ed.* **2022**, *61*, e202212542. [CrossRef] [PubMed]
97. Wu, T.; Li, S.; Liu, S.; Cheong, W.-C.; Peng, C.; Yao, K.; Li, Y.; Wang, J.; Jiang, B.; Chen, Z.; et al. Biomass-Assisted Approach for Large-Scale Construction of Multi-Functional Isolated Single-Atom Site Catalysts. *Nano Res.* **2022**, *15*, 3980–3990. [CrossRef]
98. Sun, X.; Chen, C.; Xiong, C.; Zhang, C.; Zheng, X.; Wang, J.; Gao, X.; Yu, Z.-Q.; Wu, Y. Surface Modification of MoS_2 Nanosheets by Single Ni Atom for Ultrasensitive Dopamine Detection. *Nano Res.* **2022**, *16*, 917–924. [CrossRef]
99. Ling, Y.; Ge, H.; Chen, J.; Zhang, Y.; Duan, Y.; Liang, M.; Guo, Y.; Wu, T.; Soo, Y.; Yin, X.; et al. General Strategy toward Hydrophilic Single Atom Catalysts for Efficient Selective Hydrogenation. *Adv. Sci.* **2022**, *9*, 2202144. [CrossRef]
100. Jiang, M.; Chen, X.; Wang, L.; Liang, J.; Wei, X.; Nong, W. Anchoring Single Ni Atoms on CeO_2 Nanospheres as an Efficient Catalyst for the Hydrogenolysis of Lignin to Aromatic Monomers. *Fuel* **2022**, *324*, 124499. [CrossRef]
101. Ma, R.; Gao, J.; Kou, J.; Dean, D.P.; Breckner, C.J.; Liang, K.; Zhou, B.; Miller, J.T.; Zou, G. Insights into the Nature of Selective Nickel Sites on Ni/Al_2O_3 Catalysts for Propane Dehydrogenation. *ACS Catal.* **2022**, *12*, 12607–12616. [CrossRef]
102. Bulushev, D.A.; Bulusheva, L.G. Catalysts with Single Metal Atoms for the Hydrogen Production from Formic Acid. *Catal. Rev.* **2022**, *64*, 835–874. [CrossRef]
103. Avakyan, L.A.; Manukyan, A.S.; Mirzakhanyan, A.A.; Sharoyan, E.G.; Zubavichus, Y.V.; Trigub, A.L.; Kolpacheva, N.A.; Bugaev, L.A. Atomic Structure of Nickel Phthalocyanine Probed by X-Ray Absorption Spectroscopy and Density Functional Simulations. *Opt. Spectrosc.* **2013**, *114*, 347–352. [CrossRef]
104. Jentzen, W.; Turowska-Tyrk, I.; Scheidt, W.R.; Shelnutt, J.A. Planar Solid-State and Solution Structures of (Porphinato)Nickel(II) As Determined by X-Ray Diffraction and Resonance Raman Spectroscopy. *Inorg. Chem.* **1996**, *35*, 3559–3567. [CrossRef]
105. Yamada, Y.; Suzuki, Y.; Yasuda, H.; Uchizawa, S.; Hirose-Takai, K.; Sato, Y.; Suenaga, K.; Sato, S. Functionalized Graphene Sheets Coordinating Metal Cations. *Carbon* **2014**, *75*, 81–94. [CrossRef]
106. Chernyshev, V.M.; Ananikov, V.P. Nickel and Palladium Catalysis: Stronger Demand than Ever. *ACS Catal.* **2022**, *12*, 1180–1200. [CrossRef]
107. Yang, Y.; Li, W.; Xu, H. A New Explanation for the Carbon Deposition and Elimination over Supported Ni, Ni-Ce and Ni-Co Catalysts for CO_2-Reforming of Methane. *React. Kinet. Catal. Lett.* **2002**, *77*, 155–162. [CrossRef]
108. Vogt, C.; Kranenborg, J.; Monai, M.; Weckhuysen, B.M. Structure Sensitivity in Steam and Dry Methane Reforming over Nickel: Activity and Carbon Formation. *ACS Catal.* **2020**, *10*, 1428–1438. [CrossRef]
109. Khairudin, N.F.; Sukri, M.F.F.; Khavarian, M.; Mohamed, A.R. Understanding the Performance and Mechanism of Mg-Containing Oxides as Support Catalysts in the Thermal Dry Reforming of Methane. *Beilstein J. Nanotechnol.* **2018**, *9*, 1162–1183. [CrossRef]
110. Baharudin, L.; Rahmat, N.; Othman, N.H.; Shah, N.; Syed-Hassan, S.S.A. Formation, Control, and Elimination of Carbon on Ni-Based Catalyst during CO_2 and CH_4 Conversion via Dry Reforming Process: A Review. *J. CO2 Util.* **2022**, *61*, 102050. [CrossRef]
111. Wei, J.; Iglesia, E. Isotopic and Kinetic Assessment of the Mechanism of Reactions of CH_4 with CO_2 or H_2O to Form Synthesis Gas and Carbon on Nickel Catalysts. *J. Catal.* **2004**, *224*, 370–383. [CrossRef]
112. Lustemberg, P.G.; Ramírez, P.J.; Liu, Z.; Gutiérrez, R.A.; Grinter, D.G.; Carrasco, J.; Senanayake, S.D.; Rodriguez, J.A.; Ganduglia-Pirovano, M.V. Room-Temperature Activation of Methane and Dry Re-Forming with CO_2 on Ni-CeO_2 (111) Surfaces: Effect of Ce^{3+} Sites and Metal–Support Interactions on C–H Bond Cleavage. *ACS Catal.* **2016**, *6*, 8184–8191. [CrossRef]
113. Pantha, N.; Ulman, K.; Narasimhan, S. Adsorption of Methane on Single Metal Atoms Supported on Graphene: Role of Electron Back-Donation in Binding and Activation. *J. Chem. Phys.* **2020**, *153*, 244701. [CrossRef]
114. Wu, J.; Gao, J.; Lian, S.; Li, J.; Sun, K.; Zhao, S.; Kim, Y.D.; Ren, Y.; Zhang, M.; Liu, Q.; et al. Engineering the Oxygen Vacancies Enables Ni Single-Atom Catalyst for Stable and Efficient C-H Activation. *Appl. Catal. B Environ.* **2022**, *314*, 121516. [CrossRef]
115. Akri, M.; El Kasmi, A.; Batiot-Dupeyrat, C.; Qiao, B. Highly Active and Carbon-Resistant Nickel Single-Atom Catalysts for Methane Dry Reforming. *Catalysts* **2020**, *10*, 630. [CrossRef]
116. Bellido, J.D.A.; Assaf, E.M. Effect of the Y_2O_3–ZrO_2 Support Composition on Nickel Catalyst Evaluated in Dry Reforming of Methane. *Appl. Catal. Gen.* **2009**, *352*, 179–187. [CrossRef]
117. Paladino Lino, A.V.; Rodella, C.B.; Assaf, E.M.; Assaf, J.M. Methane Tri-Reforming for Synthesis Gas Production Using Ni/$CeZrO_2$/$MgAl_2O_4$ Catalysts: Effect of Zr/Ce Molar Ratio. *Int. J. Hydrog. Energy* **2020**, *45*, 8418–8432. [CrossRef]

118. Wang, N.; Yu, X.; Shen, K.; Chu, W.; Qian, W. Synthesis, Characterization and Catalytic Performance of MgO-Coated Ni/SBA-15 Catalysts for Methane Dry Reforming to Syngas and Hydrogen. *Int. J. Hydrog. Energy* **2013**, *38*, 9718–9731. [CrossRef]
119. Zuo, Z.; Liu, S.; Wang, Z.; Liu, C.; Huang, W.; Huang, J.; Liu, P. Dry Reforming of Methane on Single-Site Ni/MgO Catalysts: Importance of Site Confinement. *ACS Catal.* **2018**, *8*, 9821–9835. [CrossRef]
120. Juan-Juan, J.; Román-Martínez, M.C.; Illán-Gómez, M.J. Effect of Potassium Content in the Activity of K-Promoted Ni/Al_2O_3 Catalysts for the Dry Reforming of Methane. *Appl. Catal. Gen.* **2006**, *301*, 9–15. [CrossRef]
121. Zapata, B.; Valenzuela, M.A.; Palacios, J.; Torres-Garcia, E. Effect of Ca, Ce or K Oxide Addition on the Activity of Ni/SiO_2 Catalysts for the Methane Decomposition Reaction. *Int. J. Hydrog. Energy* **2010**, *35*, 12091–12097. [CrossRef]
122. Kim, S.M.; Abdala, P.M.; Margossian, T.; Hosseini, D.; Foppa, L.; Armutlulu, A.; van Beek, W.; Comas-Vives, A.; Copéret, C.; Müller, C. Cooperativity and Dynamics Increase the Performance of NiFe Dry Reforming Catalysts. *J. Am. Chem. Soc.* **2017**, *139*, 1937–1949. [CrossRef]
123. Al-Fatesh, A. Suppression of Carbon Formation in CH_4–CO_2 Reforming by Addition of Sr into Bimetallic Ni–Co/γ-Al_2O_3 Catalyst. *J. King Saud Univ. Eng. Sci.* **2015**, *27*, 101–107. [CrossRef]
124. Alipour, Z.; Rezaei, M.; Meshkani, F. Effect of Alkaline Earth Promoters (MgO, CaO, and BaO) on the Activity and Coke Formation of Ni Catalysts Supported on Nanocrystalline Al_2O_3 in Dry Reforming of Methane. *J. Ind. Eng. Chem.* **2014**, *20*, 2858–2863. [CrossRef]
125. Roh, H.-S.; Jun, K.-W. Carbon Dioxide Reforming of Methane over Ni Catalysts Supported on Al_2O_3 Modified with La_2O_3, MgO, and CaO. *Catal. Surv. Asia* **2008**, *12*, 239–252. [CrossRef]
126. Ma, Q.; Sun, J.; Gao, X.; Zhang, J.; Zhao, T.; Yoneyama, Y.; Tsubaki, N. Ordered Mesoporous Alumina-Supported Bimetallic Pd–Ni Catalysts for Methane Dry Reforming Reaction. *Catal. Sci. Technol.* **2016**, *6*, 6542–6550. [CrossRef]
127. Huang, S.; Xu, H.; Li, H.; Guo, Y.; Sun, Z.; Du, Y.; Li, H.; Zhang, J.; Pang, R.; Dong, Q.; et al. Preparation and Characterization of Char Supported NiCu Nanoalloy Catalyst for Biomass Tar Cracking Together with Syngas-Rich Gas Production. *Fuel Process. Technol.* **2021**, *218*, 106858. [CrossRef]
128. Wang, Y.; Kang, L. Selective Hydrogenation of Acetylene Catalyzed by Nickel and Nitrogen-Doped C_{34}: A Density Functional Theory Study. *Chem. Phys. Lett.* **2020**, *757*, 137871. [CrossRef]
129. Poldorn, P.; Wongnongwa, Y.; Mudchimo, T.; Jungsuttiwong, S. Theoretical Insights into Catalytic CO_2 Hydrogenation over Single-Atom (Fe or Ni) Incorporated Nitrogen-Doped Graphene. *J. CO2 Util.* **2021**, *48*, 101532. [CrossRef]
130. Xue, M.; Jia, J.; Wu, H. A Density Functional Theory Study on the Catalytic Performance of Metal (Ni, Pd) Single Atom, Dimer and Trimer for H_2 Dissociation. *Chem. Phys.* **2022**, *552*, 111336. [CrossRef]
131. Zhuo, H.-Y.; Yu, X.; Yu, Q.; Xiao, H.; Zhang, X.; Li, J. Selective Hydrogenation of Acetylene on Graphene-Supported Non-Noble Metal Single-Atom Catalysts. *Sci. China Mater.* **2020**, *63*, 1741–1749. [CrossRef]
132. Sun, M.; Nelson, A.; Adjaye, J. Ab Initio DFT Study of Hydrogen Dissociation on MoS_2, NiMoS, and CoMoS: Mechanism, Kinetics, and Vibrational Frequencies. *J. Catal.* **2005**, *233*, 411–421. [CrossRef]
133. Bing, Q.; Liu, W.; Yi, W.; Liu, J. Ni Anchored C_2N Monolayers as Low-Cost and Efficient Catalysts for Hydrogen Production from Formic Acid. *J. Power Sources* **2019**, *413*, 399–407. [CrossRef]
134. Prins, R. Hydrogen Spillover. Facts and Fiction. *Chem. Rev.* **2012**, *112*, 2714–2738. [CrossRef] [PubMed]
135. Vogt, C.; Monai, M.; Kramer, G.J.; Weckhuysen, B.M. The Renaissance of the Sabatier Reaction and Its Applications on Earth and in Space. *Nat. Catal.* **2019**, *2*, 188–197. [CrossRef]
136. Sun, J.; Zhao, H.; Fang, X.; Zhai, S.; Zhai, D.; Sun, L.; Deng, W. Theoretical Studies on the Catalytic Hydrogenation of Carbon Dioxide by 3d Transition Metals Single-Atom Catalyst Supported on Covalent Triazine Frameworks. *Mol. Catal.* **2021**, *508*, 111581. [CrossRef]
137. Homlamai, K.; Maihom, T.; Choomwattana, S.; Sawangphruk, M.; Limtrakul, J. Single-Atoms Supported (Fe, Co, Ni, Cu) on Graphitic Carbon Nitride for CO_2 Adsorption and Hydrogenation to Formic Acid: First-Principles Insights. *Appl. Surf. Sci.* **2020**, *499*, 143928. [CrossRef]
138. Esrafili, M.D.; Sharifi, F.; Dinparast, L. Catalytic Hydrogenation of CO_2 over Pt- and Ni-Doped Graphene: A Comparative DFT Study. *J. Mol. Graph. Model.* **2017**, *77*, 143–152. [CrossRef]
139. Ren, Y.; Sun, X.; Qi, K.; Zhao, Z. Single Atom Supported on MoS_2 as Efficient Electrocatalysts for the CO_2 Reduction Reaction: A DFT Study. *Appl. Surf. Sci.* **2022**, *602*, 154211. [CrossRef]
140. Alonso, G.; López, E.; Huarte-Larrañaga, F.; Sayós, R.; Prats, H.; Gamallo, P. Zeolite-Encapsulated Single-Atom Catalysts for Efficient CO_2 Conversion. *J. CO2 Util.* **2021**, *54*, 101777. [CrossRef]
141. Zhang, Z.; Shen, C.; Sun, K.; Jia, X.; Ye, J.; Liu, C. Advances in Studies of the Structural Effects of Supported Ni Catalysts for CO_2 Hydrogenation: From Nanoparticle to Single Atom Catalyst. *J. Mater. Chem. A* **2022**, *10*, 5792–5812. [CrossRef]
142. Millet, M.-M.; Algara-Siller, G.; Wrabetz, S.; Mazheika, A.; Girgsdies, F.; Teschner, D.; Seitz, F.; Tarasov, A.; Levchenko, S.V.; Schlögl, R.; et al. Ni Single Atom Catalysts for CO_2 Activation. *J. Am. Chem. Soc.* **2019**, *141*, 2451–2461. [CrossRef]
143. Farlow, M.W.; Adkins, H. The Hydrogenation of Carbon Dioxide and a Correction of the Reported Synthesis of Urethans. *J. Am. Chem. Soc.* **1935**, *57*, 2222–2223. [CrossRef]
144. Wang, T.; Ren, D.; Huo, Z.; Song, Z.; Jin, F.; Chen, M.; Chen, L. A Nanoporous Nickel Catalyst for Selective Hydrogenation of Carbonates into Formic Acid in Water. *Green Chem.* **2017**, *19*, 716–721. [CrossRef]

145. Cen, Y.; Yue, Y.; Wang, S.; Lu, J.; Wang, B.; Jin, C.; Guo, L.; Hu, Z.-T.; Zhao, J. Adsorption Behavior and Electron Structure Engineering of Pd-Based Catalysts for Acetylene Hydrochlorination. *Catalysts* **2019**, *10*, 24. [CrossRef]
146. Riley, C.; Zhou, S.; Kunwar, D.; De La Riva, A.; Peterson, E.; Payne, R.; Gao, L.; Lin, S.; Guo, H.; Datye, A. Design of Effective Catalysts for Selective Alkyne Hydrogenation by Doping of Ceria with a Single-Atom Promotor. *J. Am. Chem. Soc.* **2018**, *140*, 12964–12973. [CrossRef] [PubMed]
147. Dai, X.; Chen, Z.; Yao, T.; Zheng, L.; Lin, Y.; Liu, W.; Ju, H.; Zhu, J.; Hong, X.; Wei, S.; et al. Single Ni Sites Distributed on N-Doped Carbon for Selective Hydrogenation of Acetylene. *Chem Commun* **2017**, *53*, 11568–11571. [CrossRef] [PubMed]
148. Ning, L.; Liao, S.; Li, H.; Tong, R.; Dong, C.; Zhang, M.; Gu, W.; Liu, X. Carbon-Based Materials with Tunable Morphology Confined Ni(0) and Ni-N_x Active Sites: Highly Efficient Selective Hydrogenation Catalysts. *Carbon* **2019**, *154*, 48–57. [CrossRef]
149. Wang, F.-F.; Guo, R.; Jian, C.; Zhang, W.; Xue, R.; Chen, D.-L.; Zhang, F.; Zhu, W. Mechanism of Catalytic Transfer Hydrogenation for Furfural Using Single Ni Atom Catalysts Anchored to Nitrogen-Doped Graphene Sheets. *Inorg. Chem.* **2022**, *61*, 9138–9146. [CrossRef]
150. Bulushev, D.A.; Ross, J.R.H. Towards Sustainable Production of Formic Acid. *ChemSusChem* **2018**, *11*, 821–836. [CrossRef]
151. Gharib, A.; Arab, A. Decomposition of Formic Acid via Carboxyl Mechanism on the Graphene Nanosheet Decorated by Cr, Mn, Fe, Co, Ni, Pd, Ag, and Cd Metals: A DFT Study. *Int. J. Hydrog. Energy* **2023**, *48*, 566–575. [CrossRef]
152. Akça, A.; Karaman, O. Electrocatalytic Decomposition of Formic Acid Catalyzed by M-Embedded Graphene (M = Ni and Cu): A DFT Study. *Top. Catal.* **2022**, *65*, 1–13. [CrossRef]
153. Bing, Q.; Liu, J. Transition Metal Single Atom Anchored C_3N for Highly Efficient Formic Acid Dehydrogenation: A DFT Study. *Appl. Surf. Sci.* **2021**, *562*, 150186. [CrossRef]
154. Zhong, W.; Liu, Y.; Deng, M.; Zhang, Y.; Jia, C.; Prezhdo, O.V.; Yuan, J.; Jiang, J. C_2N-Supported Single Metal Ion Catalysts for HCOOH Dehydrogenation. *J. Mater. Chem. A* **2018**, *6*, 11105–11112. [CrossRef]
155. Feng, B.; Guo, R.; Cai, Q.; Song, Y.; Li, N.; Fu, Y.; Chen, D.-L.; Zhang, J.; Zhu, W.; Zhang, F. Construction of Isolated Ni Sites on Nitrogen-Doped Hollow Carbon Spheres with Ni–N_3 Configuration for Enhanced Reduction of Nitroarenes. *Nano Res.* **2022**, *15*, 6001–6009. [CrossRef]
156. Genç, A.E.; Küçük, H.; Alp, I.O.; Akça, A. Hydrazine Decomposition on Nickel-Embedded Graphene. *Int. J. Hydrog. Energy* **2020**, *45*, 33407–33418. [CrossRef]